Consequences of the force-free model of magnetic clouds for their heliospheric evolution

M. Leitner,[1,2] C. J. Farrugia,[3] C. Möstl,[1,2] K. W. Ogilvie,[4] A. B. Galvin,[3] R. Schwenn,[5] and H. K. Biernat[1,2]

Received 28 June 2006; revised 25 February 2007; accepted 3 April 2007; published 22 June 2007.

[1] We examine the implications of the widely used, force-free, constant-α flux rope model of interplanetary magnetic clouds for the evolution of these mesoscale (fraction 1 AU) structures in the heliosphere, with special emphasis on the inner ($\leq$1 AU) heliosphere. We employ primarily events observed by the Helios 1 and 2 probes between 0.3 and 1 AU in the ascending and maximum phases of solar cycle 21 and by Wind at 1 AU in a similar phase of solar activity cycle. We supplement these data by observations from other spacecraft (e.g., Voyagers 1 and 2, Pioneers 10 and 11, and others). Our data set consists of 130 events. We explore three different approaches. In the first, we work with ensemble averages, binning the results into radial segments of width 0.1 AU in the range $0.3 \leq r_h \leq 1$ AU. Doing this, we find that in the inner heliosphere the modeled average central axial field strength, $\langle B_0 \rangle$, varies with heliospheric distance r_h as $\langle B_0 \rangle$ [nT] = $18.1 \cdot r_h^{-1.64}$ [AU], and the average diameter increases quasi-linearly as $\langle D \rangle$ [AU] = $0.23\ r_h^{1.14}$. The orientation of the axis of the underlying magnetic flux tube in our data set is generally found to lie along the east–west direction and in the ecliptic plane at all values of r_h, but there is considerable scatter about these average directions. In the second, we monitor the evolution of magnetic clouds in snapshot fashion, using seven spacecraft alignments. The results are in broad agreement with the statistics reported under step 1. In the final approach, we obtain the functional dependence of B_0 and D predicted by an analytic expression for a freely expanding Lundquist flux tube. We find D to vary linearly with r_h, broadly similar to that obtained under approach 1. The maximum field strength scales as r_h^{-2} compared to a $r_h^{-1.3}$ dependence obtained from statistics. We compare our findings with those of Bothmer and Schwenn (1998), who used a different methodology. The results obtained form a good background to the forthcoming Solar Terrestrial Relations Observatory (STEREO) and Sentinels missions and to multispacecraft studies of magnetic clouds.

Citation: Leitner, M., C. J. Farrugia, C. Möstl, K. W. Ogilvie, A. B. Galvin, R. Schwenn, and H. K. Biernat (2007), Consequences of the force-free model of magnetic clouds for their heliospheric evolution, *J. Geophys. Res.*, *112*, A06113, doi:10.1029/2006JA011940.

1. Introduction

[2] The Helios 1 and 2 data sets covering the period 1974–1981, corresponding to the rising phase and solar activity maximum of solar cycle 21, are a valuable resource for understanding inner-heliospheric processes (see review by *Schwenn* [1983]). In particular, one can obtain how the parameters of strongly geoeffective interplanetary configurations, such as magnetic clouds (MCs), scale with heliospheric distance, an important input to space weather studies. With the Helios data sets, *Bothmer and Schwenn* [1996, 1998] investigated the origin and structure of MCs in the inner heliosphere.

[3] Using observations at 1 AU, *Burlaga et al.* [1981] defined MCs as structures in which a magnetic field of enhanced strength rotates through a large angle in a plasma of low proton β and temperature. These defining criteria were shown to hold also for MCs in inner heliosphere by *Bothmer and Schwenn* [1998]. Further, these authors advanced evidence in support of the flux tube model for these ejecta. Using several lineups of the Helios, Voyager, and IMP spacecraft, they also obtained direct evidence for the radial expansion of magnetic clouds, first postulated by *Klein and Burlaga* [1982]. Further, they correlated obser-

[1]Space Research Institute, Austrian Academy of Sciences, Graz, Austria.
[2]Institute of Physics, University of Graz, Graz, Austria.
[3]Space Science Center and Department of Physics, University of New Hampshire, Durham, New Hampshire, USA.
[4]Laboratory for Extraterrestrial Physics, NASA Goddard Space Flight Center, Greenbelt, Maryland, USA.
[5]Max Planck Institute for Solar System Research, Katlenburg-Lindau, Germany.

Copyright 2007 by the American Geophysical Union.
0148-0227/07/2006JA011940

vations about the orientation and helicity of Helios MCs with similar properties of disappearing filaments on the Sun.

[4] The orientation of the flux rope axis was obtained in that study by minimum variance analysis (MV) [*Sonnerup and Cahill*, 1967], in which the orientation of the axis is given by the intermediate vector (i.e., that associated with the intermediate eigenvalue [see also *Goldstein*, 1983]). The orientation is, of course, of central importance because it is a major factor determining the strength and duration of IMF B_z, as shown by *Zhao and Hoeksema* [1998] and *Zhao et al.* [2001]. (Other factors include the properties of the source region and the effect of heliospheric modulation.)

[5] The aim of this paper is to see what implications a widely used model for magnetic clouds has on the evolution of these structures. The main emphasis is statistical. We shall model magnetic clouds and obtain relevant parameters by least squares fitting the data to a force-free, cylindrically symmetric, constant-α configuration, i.e., as a cylindrically symmetric solution of $\nabla \times \mathbf{B} = \alpha \mathbf{B}$. We obtain the scaling with heliospheric distance of the modeled magnetic field strength, the radius of the tube, and the orientation of the flux tube axis. Further investigated parameters, which are not linked with the fit results, are average proton densities and temperatures, the plasma β and the solar wind "quasi-invariant," which gives the ratio of the magnetic energy density to the plasma kinetic energy density [*Osherovich et al.*, 1999]. We then interpret the results. With spacecraft lineups, i.e., observations made by two or more spacecraft located at different heliospheric distances and intercepting the same cloud at different times, we confirm and extend the statistical results we obtained in the inner heliosphere. Finally, we derive predictions on MC evolution from a theoretical model of expanding MCs. Where appropriate, comparison with the results of *Bothmer and Schwenn* [1998] and others are briefly discussed.

2. Force-Free Magnetic Field Model

[6] We follow the model first proposed by *Burlaga* [1988] and elaborated by *Lepping et al.* [1990] and consider a given magnetic cloud as a force-free, constant-α magnetic field configuration with a locally straight cylindrical geometry of circular cross section. The solution in cylindrical coordinates is a two-component magnetic field first given by *Lundquist* [1950]. The axial component is given by $B_a = B_0 J_0(\alpha R)$, and the azimuthal component is given by $B_\phi = H B_0 J_1(\alpha R)$, where B_0 is the maximum magnetic field strength, which is reached on the axis of the magnetic flux tube; J_0 and J_1 are the Bessel functions of zeroth and first order; α is a constant given by $\alpha = 2.4/R_0$, with R_0 the radius of the cylinder; R the radial distance from the axis of the cylinder $0 \leq R \leq R_0$; and H the magnetic helicity, with $H = \pm 1$.

[7] Least squares fitting of the observed components of the magnetic field to the model is carried out to reproduce the magnetic field geometry as observed by the spacecraft, i.e., minimizing quantity χ which is given by $\chi^2 = [\Sigma_{i=1}^{3} (B_i^O - B_i^M)^2]/(B_0 \cdot N)$, where O and M denote the observed and the model values, respectively, and N is the number of data points. The procedure results in the following fitted parameters: B_0, the field strength on the MC axis; angles θ and ϕ, the latitude and longitude of the axis of the cylinder; the parameter Y_0, which sets the trajectory through the structure as a line parallel to the x-axis in the Solar Ecliptic (SE) coordinate system given by $y = Y_0$; and H, the helicity of the MC. From these values there results the closest distance ("impact parameter", p) at which the spacecraft passes from the axis of the cloud, $0 \leq p \leq R_0$, which, in combination with the orientation, gives the size (diameter, D) of the MC.

[8] In Figures 1–3 we give three examples to illustrate the quality of the fits we obtain. The three MCs were observed at different heliospheric distances. In each of these figures we show from top to bottom the total magnetic field strength and its components in SE coordinates, the proton bulk speed, number density and temperature, and the plasma β based on the protons. The MC interval is delimited by the last two dotted vertical guidelines. The red traces reproduce the solution obtained from the fitting routine. The red trace in the temperature panel gives the expected temperature for normal solar wind expansion as derived in the statistical studies of *Lopez and Freeman* [1986].

[9] In Figure 1 a magnetic cloud is observed by the spacecraft Helios 1 on day of year (DOY) 63–64 in 1975, when the spacecraft is situated at 0.39 AU. Between the vertical lines, all the defining criteria of a magnetic cloud are satisfied. (For further details on this event the reader is referred to *Bothmer and Schwenn* [1998].) The cloud did not drive a shock. (For properties of slow magnetic clouds the reader is referred to *Tsurutani et al.* [2004].) The result of the fit is $B_0 = 63$ nT, $\phi = 118.8°$, $\theta = 2.1°$, $p = 0.00$, $H = -1$. The model gives good agreement in the amplitude and temporal profiles of B_y and B_z but does not reproduce the B_x component well. The total field maximizes at the rear of the interval, possibly as a result of compression from the trailing high-speed stream. In the Lundquist solution, of course, the field strength maximizes at the center, at twice its value at the boundaries.

[10] Figure 2 shows an example observed by Helios 1 on DOY 172 in 1980, when the spacecraft is at 0.52 AU (For more details, see also *Burlaga et al.* [1982] and *Bothmer and Schwenn* [1998]). The additional third vertical guideline marks the arrival of the shock driven by this ejecta. The result of the least squares fit is $B_0 = 48.4$ nT, $\phi = -99.2°$, $\theta = 10.0°$, $p = 0.17$, $H = -1$. While the behavior of the magnetic field components are reproduced quite well by the force-free model, a large deviation is evident in the total magnetic field strength, a common feature of these fits [see *Lepping et al.*, 1990]. The continuously declining field strength may be due to expansion effects, which are not addressed by the static force-free field model.

[11] In Figure 3 another MC observation from Helios 1, made on DOY 240–241, 1977, is shown, when the spacecraft is situated at 0.85 AU. (Other details on this event have been published by *Bothmer and Schwenn* [1998].) Again the event drives a shock (first vertical guideline) and the MC interval lies between the second and third vertical guideline. The result from the fit is $B_0 = 32.8$ nT, $\phi = 108.5°$, $\theta = 12.6°$, $p = 0.31$, $H = -1$. The behavior of the y and z components is reproduced well, and the largest deviation from the data occurs in the first hours of the MC observation. The x component of the field switches polarity from small negative to small positive values, a feature which the fit does not reproduce. However, compared to the other two components, this signature is much

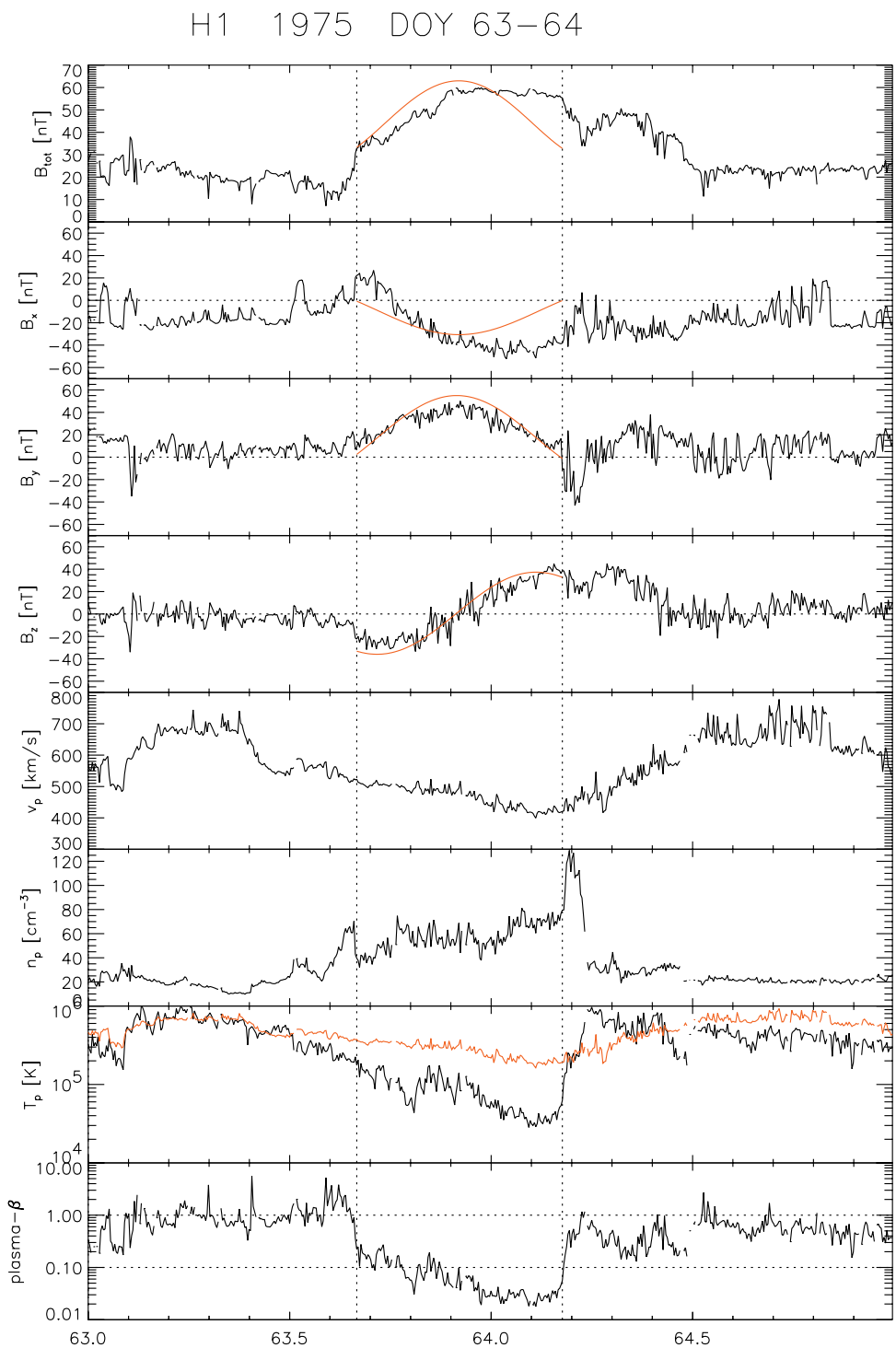

Figure 1. Observation of a magnetic cloud by Helios 1 at 0.39 AU.

smaller, and on average the fit is between this magnetic field change.

3. Statistical Survey

3.1. Data Selection Criteria

[12] The data set consists of all Helios 1 and 2 MCs tabulated by *Bothmer and Schwenn* [1998] provided the least squares fit gives reliable results, i.e., there are few data gaps, and data resolution is good enough for fitting; the rotation of the magnetic field is reproduced well; and, overall, a visual inspection shows that the fit describes the behavior of the observations well. Most of the events are observed between 0.3 and 1 AU in the rising part of solar cycle 21 and we end up with 43 events from Helios. We also took a selection of MCs seen by Wind in the years 1995–2000, i.e., in a phase of the present solar cycle similar of that when the Helios data we use were acquired, but two

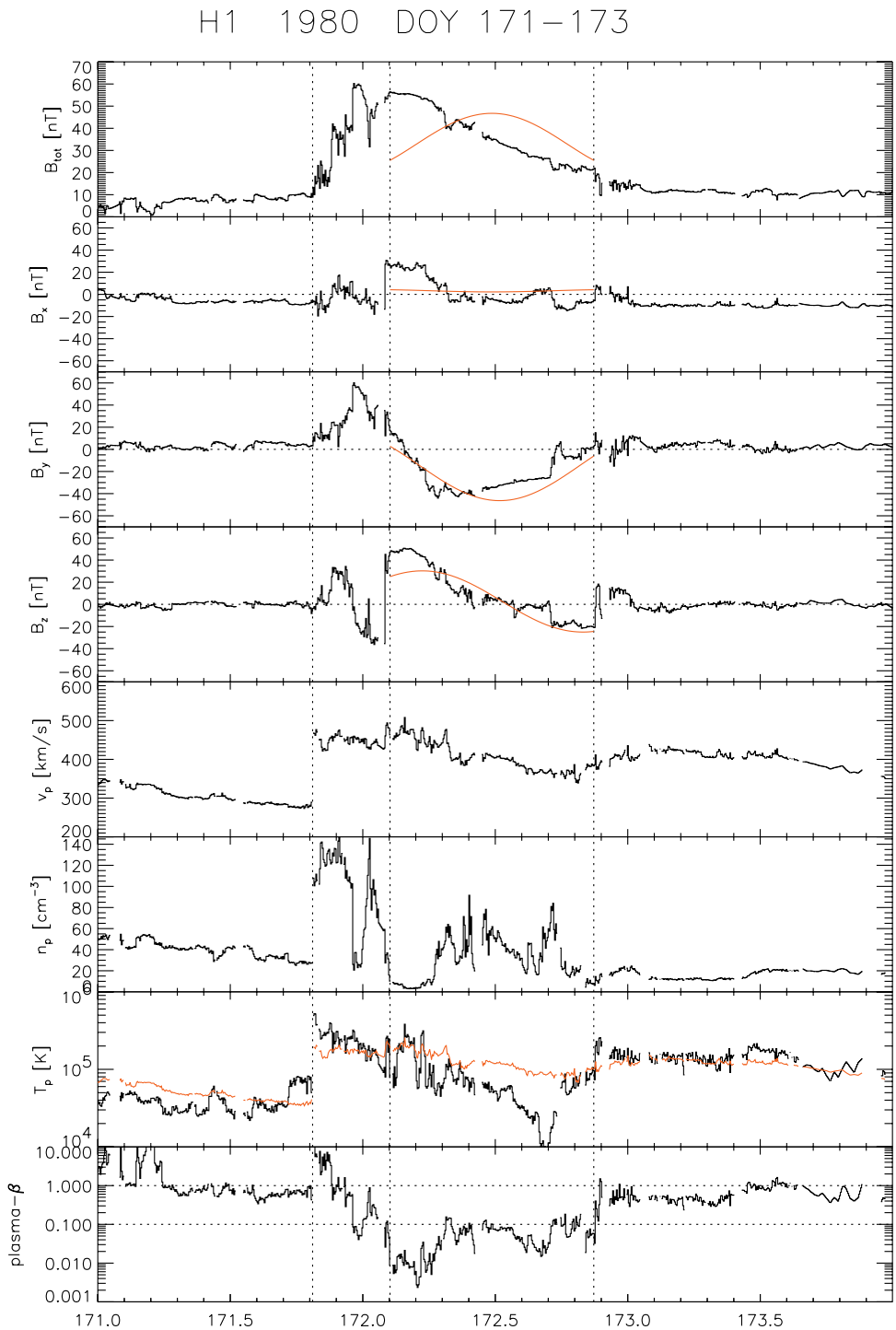

Figure 2. Observation of a magnetic cloud by Helios 1 at 0.52 AU.

solar cycles later. More events at 1 AU are provided by ISEE-3 and IMP-8, whose operating periods overlapped that of Helios.

[13] MC observations made by the Pioneer Venus orbiter (PVO) gives us further values at 0.72 AU. Magnetic cloud observations beyond 1 AU are acquired by Pioneer 10 (P10), Pioneer 11 (P11), Voyager 1 (V1), and Voyager 2 (V2). This allows us to include observations spanning a wide range of heliospheric distances. However, partly because the inner-heliospheric ($\leq$1 AU) coverage is more dense and partly because these are the data of direct relevance to geospace, we give separate results for this range. The frequency of solar mass ejections, and as a consequence of MCs, depends on the solar cycle [e.g., *Howard et al.*, 1986; *Webb and Howard*, 1994; *Huttunen et al.*, 2005], but for this study we are not investigating any solar cycle effects on the investigated parameters.

[14] The initial data set consists of 159 MCs. We then apply two selection criteria. We exclude all those cases where (1) either the MCs are intersected too far away from

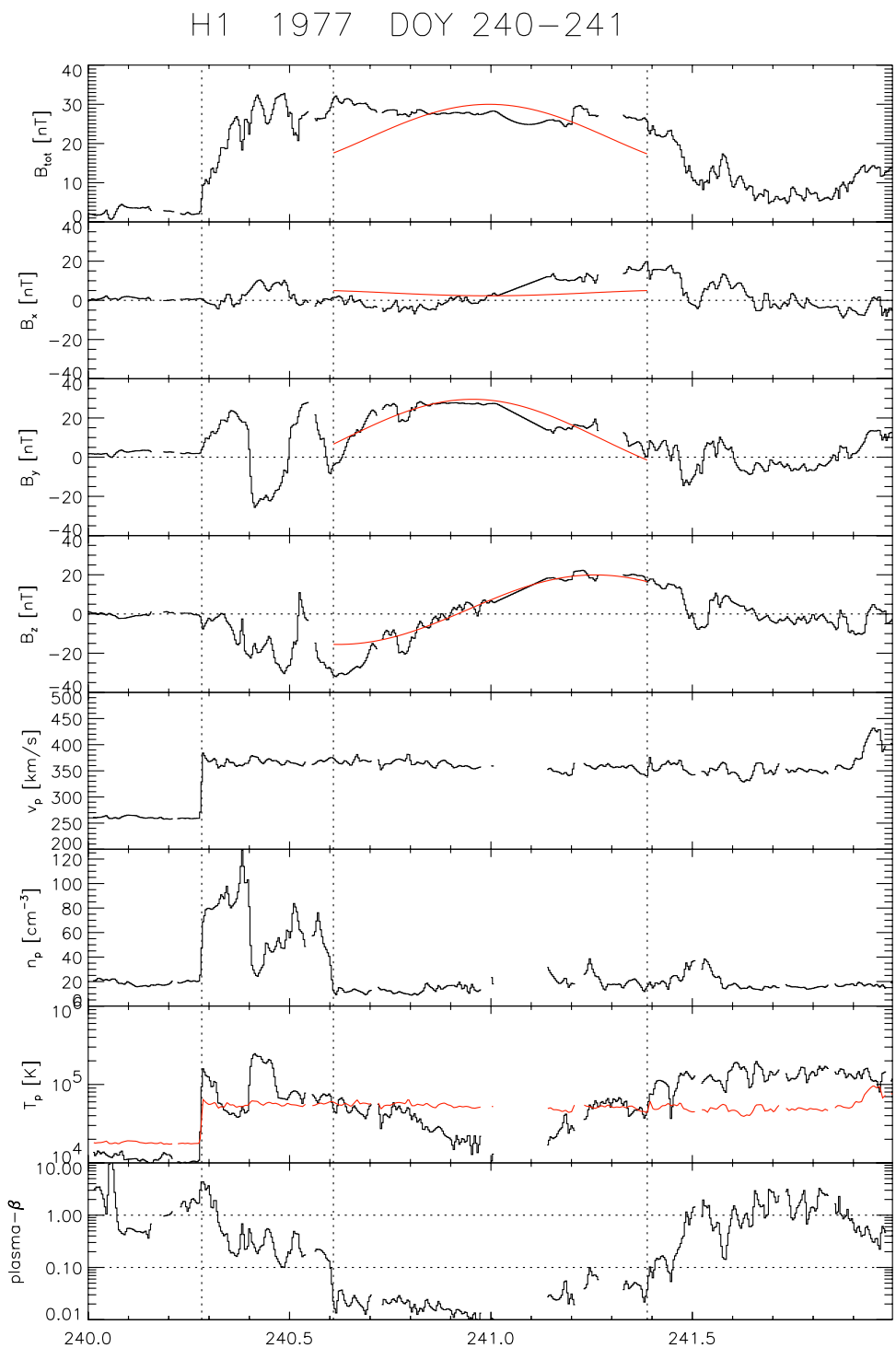

Figure 3. Observation of a magnetic cloud by Helios 1 at 0.85 AU.

the center, $p > 0.7\ R_0$, or (2) the inferred orientation of the flux tube can lead to problematic cuts of the intersection line through the cylinder, for example, if the cloud axis is oriented almost parallel to the x-axis. These latter are represented by the dotted areas in Figure 5, where they are shown as orientations lying within a cone about the x-axis of angular width $\phi = \pm 30°$, and $\theta = \pm 30°$ above or below the ecliptic plane. In total, 29 events were excluded based on one or both of these criteria so that our final data set consists of 130 events.

[15] For the statistical part of the work we use ensemble averages. We group the events within radial bins as described in the caption to Figure 4, which shows the distribution of the MCs in our survey as a function of heliospheric distance, r_h. Within each bin and for each of the investigated parameters the mean value and standard deviation (σ) are determined. To these values a power

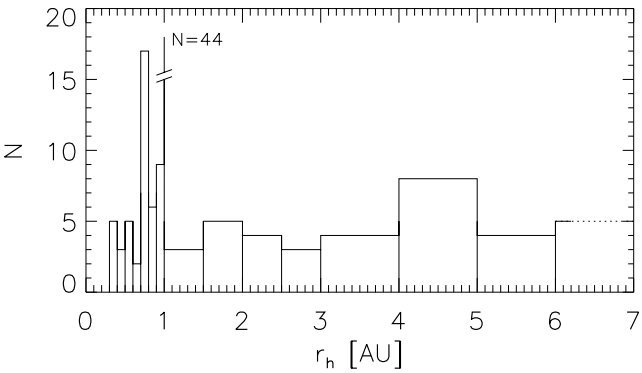

Figure 4. Distribution of the 130 MC events in each chosen r_h-bin. Observations at 1 AU are mainly from Wind (some from ISEE-3 and IMP-8) are grouped separately (44 events). For distances bigger than 6 AU all events are grouped together.

law ($y = a \cdot r_h^b$) is fitted, which is weighted by the determined standard deviation ($w = 1/\sigma^2$).

3.2. Statistical Results

3.2.1. Orientation

[16] From the fit routine we obtain the two angles θ and ϕ, which determine the orientation of the MC axis in SE coordinates. The distribution of the axis orientation is shown in the overview Figure 5, which is a projection of the two angles on a sphere. Looking from above on the ecliptic plane the x-axis points toward the Sun, the z-axis points from the center out of the plane, and the y-axis completes the SE coordinate system. In this representation, the MC axis points from the center to the given points, where plus signs indicate orientations above the ecliptic plane and diamonds symbols indicate those below the ecliptic plane.

[17] Figure 6 gives the distribution of the angles ϕ (on the left) and θ for all the 130 events. (As a word of caution, note that in this kind of presentation the number of events tends to appear smaller for larger θ.) For the angle ϕ we examine the difference to the y-axis, therefore ϕ values greater than 180° are mirrored through the center to the interval $0° \leq \phi \leq 180°$. The overall preferred direction of the flux tube axis is to point along the y-axis with a small deviation from it, the average value and standard deviation being $\langle\phi\rangle = 92° \pm 37°$. The values of θ are grouped around the ecliptic plane, which is the horizontal line in the figure, with an average preference somewhat south of the ecliptic plane. Most of the events were found with an angle θ not directly in the ecliptic plane but slightly below it, the average value and standard deviation being $\langle\theta\rangle = -4° \pm 28°$.

[18] The variation of $\langle\phi\rangle$ and $\langle\theta\rangle$ with heliospheric distance is shown in Figure 7. There appears to be a tendency for $\langle\phi\rangle$ to vary quite substantially in the inner heliosphere, whereas with increasing distances $\langle\phi\rangle$ varies little around 90°. (However, recall that the statistics are poor for $r_h > 2$ AU.) The variations of the average $\langle\theta\rangle$ values are similar to those for $\langle\phi\rangle$: a trend for large departures from the ecliptic plane is seen in the inner heliosphere, while the axes lie mainly in the ecliptic plane for larger distances. We may relate these results to other studies. Most relevant to our work, because they cover the same period, is the work of *Bothmer and Schwenn* [1998] and *Lepping et al.* [1990]. *Bothmer and Schwenn* [1998] found that there are indications of an overabundance of flux tube axes orientations in the range 10° south to 10° north, i.e., with low inclinations to the ecliptic. As regards the azimuthal direction, the cloud axes were found in that study to scatter about the east–west direction, with an average azimuth of 91° (rms = 44°). *Lepping et al.* [1990] surveyed 18 clouds in the time interval 1967–1982, i.e., overlapping our period. The most probable direction of the cloud's axis was within 15° of the ecliptic plane and ~100° from the Sun's direction when it is projected into the ecliptic plane. However, they note that a broad range is observed. *Bothmer* [2003] examined five clouds in the years 1997–2000, with emphasis on the geoeffects they elicited. Of these, minimum variance analysis showed that three were highly inclined to the ecliptic. *Huttunen et al.* [2005] examined an extensive selection of magnetic clouds in solar cycle 23 spanning the years 1997–2003 (ascending, maximum, and descending phases). They found that highly inclined clouds occurred frequently in the declining phase but were also present in the ascending phase.

3.2.2. Central Axial Magnetic Field Strength

[19] Comparing the averaged magnetic field strength $\langle B_{tot}\rangle$ inside each MC with the fitted magnetic field strength B_0, it is found that $B_0 = 1.35\ \langle B_{tot}\rangle$. For the peak observed field the relation is $B_0 = 1.13\ B_{\max}$. If the difference between

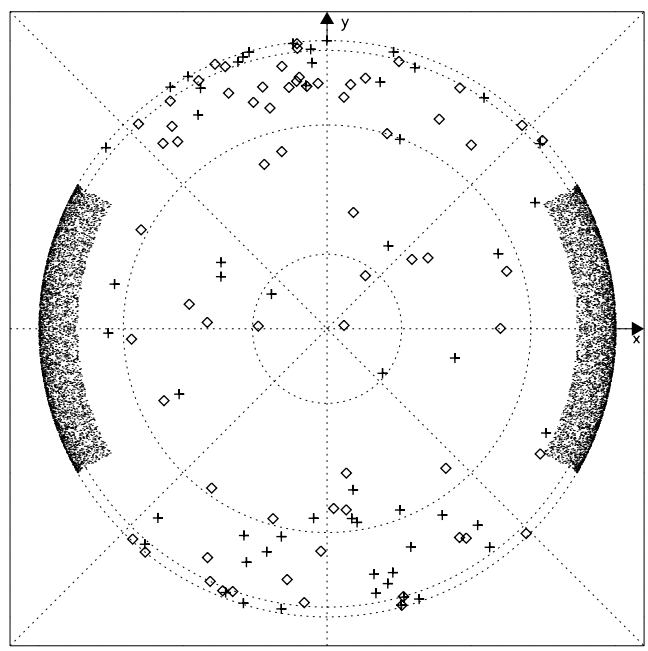

Figure 5. The orientation of the magnetic cloud axes, given by the angles θ and ϕ, in a solar ecliptic coordinate system (x points toward the Sun, and x-y plane is the ecliptic plane). Dotted circles are for $\theta = 0°$ (outermost), 15°, 45° and 75°. Here $\theta = 90°$ is at the center. Plus signs refer to MC axes pointing above the ecliptic plane and diamond symbols refer to orientations below the ecliptic plane. Fit result with orientations within the two shaded areas (small θ and $-30° \leq \phi \leq 30°$) give unreliable fits and are excluded from further analysis.

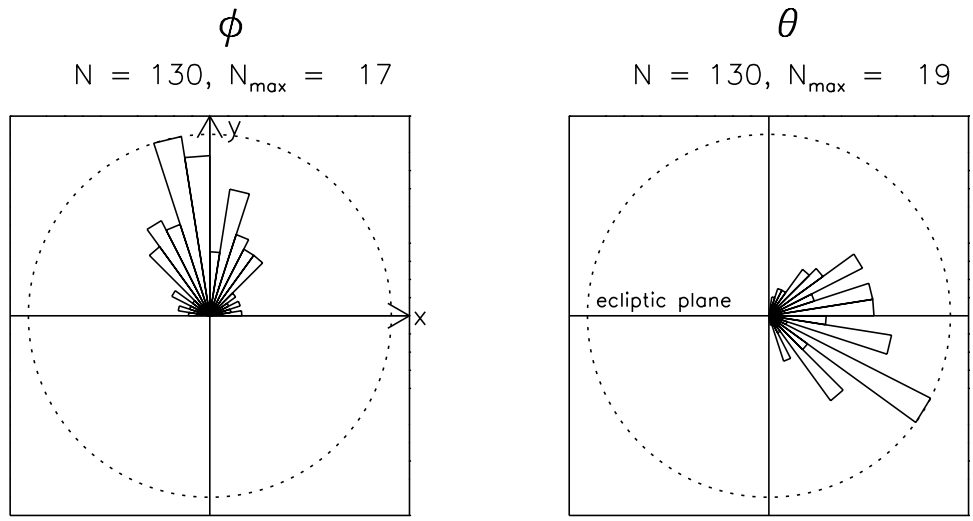

Figure 6. Distribution of the angle ϕ with respect to the y-axis and the angle θ with respect to the ecliptic plane.

data and fit result is compared with the impact parameter p, the difference is smaller for trajectories close to the center, which is in agreement with the model assumptions.

[20] The behavior of $\langle B_0 \rangle$ as a function of heliospheric distance, r_h, is shown in Figure 8, where the large plot gives this behavior for all r_h, and the inset shows our results for the inner heliosphere. The solid lines are fits of the type $y = a \cdot r_h^b$, which are weighted by the inverse squared standard deviation $w = 1/\sigma^2$ (Gaussian weighting). We used the numerical algorithm "curvefit" from Numerical Recipes [*Press et al.*, 1982], which returns the values of a and b and their error bars calculated as standard deviations. The routine converged and, for the whole range of r_h, it yielded (B_0 in nT and r_h in AU),

$$\langle B_0 \rangle = (18.8 \pm 1.4) \cdot r_h^{(-1.30 \pm 0.09)}, \tag{1}$$

while for the inner heliosphere alone we have

$$\langle B_0 \rangle = (18.1 \pm 3.8) \cdot r_h^{(-1.64 \pm 0.40)}. \tag{2}$$

[21] A word of caution on this and similar formulae quoted in this section is in order. The standard deviations in the fits do not exactly reflect the variability in a given r_h bin, although they lie in the same order of magnitude. Thus to take an extreme example, for $r_h = 0.65$ AU, equation (2) gives a nominal value for $\langle B_0 \rangle$ of 37 nT and a range between 24 and 53 nT, while Figure 1 gives 40 ± 25 nT. We should also note that the variability in the fits stems from the variability in both parameters a and b.

[22] In the large plot, a kink in the profile appears at about $r_h = 2$ AU, suggesting that for $r_h > 2$ AU, $\langle B_0 \rangle$ decreases less rapidly than in the inner heliosphere. This may be a spurious result due to poor statistics for high r_h. If so, this can be remedied by taking more events, which is beyond the scope of this paper. However, its cause may be more fundamental. In past work on a self-similarly expanding flux rope model, it was argued that the axial and azimuthal components of the flux rope field scale differently with r_h, the axial field B_a decreasing as $B_a \propto 1/r_h^2$, and the azimuthal field as $B_\phi \propto 1/r_h$ [e.g., *Osherovich et al.*, 1993; *Farrugia et al.*, 1993b]. In this model therefore, as time from ejection at the Sun (and r_h) passes, the decline in B_0 becomes increasingly determined by that of B_ϕ, leading to a slower decrease at large r_h. This might be the cause of the kink. If we just fit the values beyond 1 AU (dashed line), the result is

$$\langle B_0 \rangle = (11.1 \pm 3.4) \cdot r_h^{(-0.88 \pm 0.22)}. \tag{3}$$

[23] Using 12-hour average values of the magnetic field strength, *Mariani and Neubauer* [1990] found that in the inner heliosphere the IMF strength decreases as $\langle B \rangle = (3.85 \pm 0.24) r_h^{(-1.56 \pm 0.09)}$ for Helios 1 and as $\langle B \rangle = (3.29 \pm 0.17) r_h^{(-1.84 \pm 0.08)}$ for Helios 2. (If separated into high-speed (>550 km s^{-1}) and low-speed solar winds, they obtain exponents of −1.86 and −1.64, respectively.) Taking an average of the Helios 1 and 2 results and comparing with our result for the inner heliosphere (equation (2)) we find $\langle B_0 \rangle_{MC} / B_{IMF} = 5.0 r_h^{0.06}$, a weak function of r_h which increases from 4.6 at 0.3 AU to 5.0 at 1 AU.

3.2.3. Average Diameter of Magnetic Flux Tube

[24] We next discuss the average diameter, $\langle D \rangle$, of the MC flux ropes in our survey as a function of r_h. To determine $\langle D \rangle$, we stay within the assumptions of the model as described above. The structure is regarded as a straight cylinder of circular cross section, which is intersected by the spacecraft in a way revealed by the least squares fit routine in the impact parameter p. Using the fit results on the orientation of the flux tube and the impact parameter, p, we can transform the measured distances into diameters of the magnetic cloud as follows. The axis of the cloud and the spacecraft trajectory relative to the cloud form two skew lines whose closest approach is p, the impact parameter. The displacement vector of the spacecraft with respect to the cloud is $V_{MC} \cdot t \cdot \hat{\mathbf{x}}$, where V_{MC} is the, assumed constant, speed of the cloud, $\hat{\mathbf{x}}$ is a unit vector along X (SE coordinates), and t is the time spent crossing the ejection.

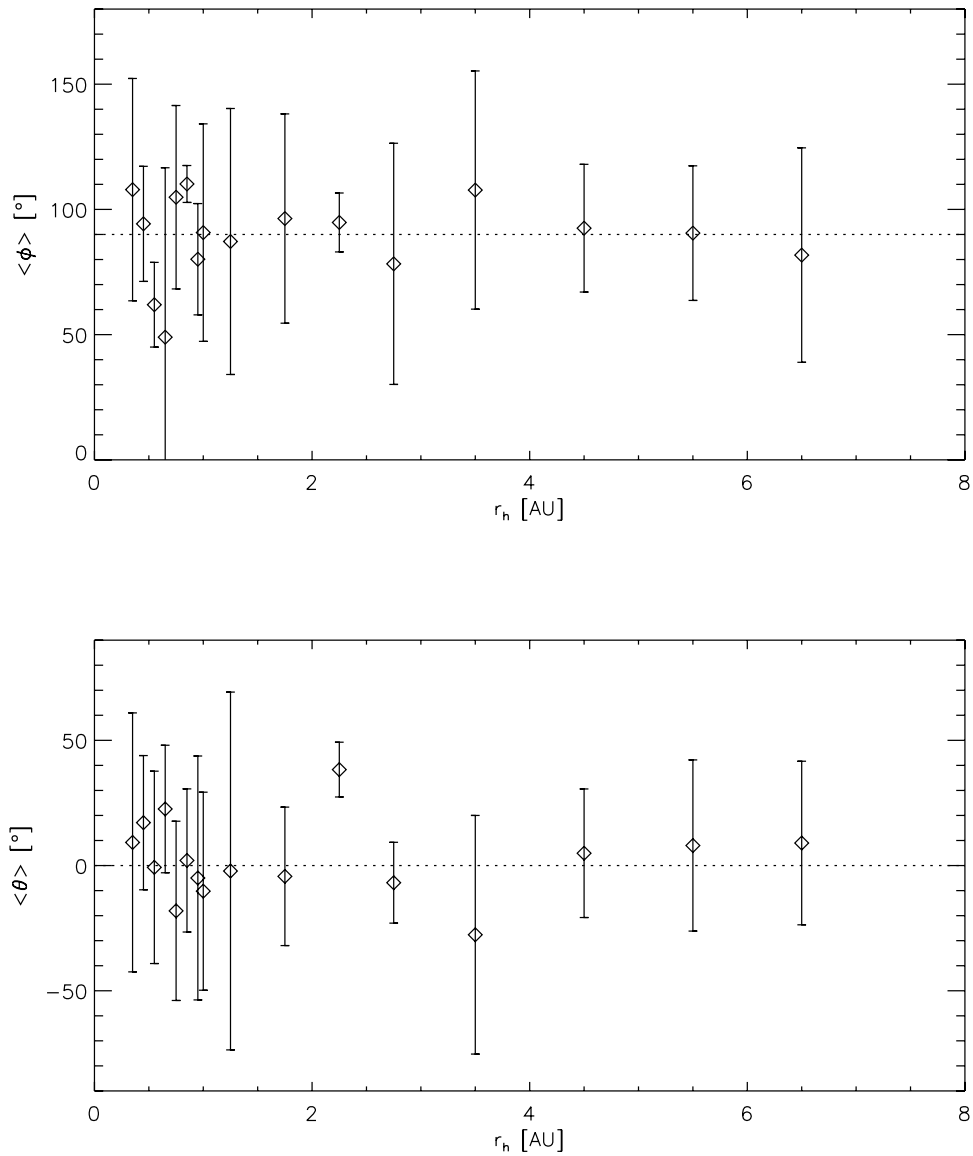

Figure 7. Variations of the average angles ϕ and θ with heliospheric distance. The dotted line in the ϕ panel gives the orientation of the y-axis ($\phi = 90°$) and in the θ panel it marks the ecliptic plane $\theta = 0°$.

A unit vector along the cloud axis, which is oriented at (θ, ϕ), is $(\cos\theta\cos\phi, \cos\theta\sin\phi, \sin\theta) \equiv (\cos\xi, \cos\theta\sin\phi, \sin\theta)$, where ξ is the angle between the cloud axis and spacecraft displacement vector. Therefore the distance travelled by the spacecraft in a direction perpendicular to the cloud axis is $\Sigma = V_{MC} \cdot t \cdot \sin\xi$. Using the impact parameter p, simple trigonometry then shows that the diameter, D, of the magnetic cloud is given by $D = \Sigma/\sin[a\tan(\Sigma/2p)]$. In summary, the evaluation of $\langle D \rangle$ involves both the force-free model as well as the underlying geometrical assumptions, particularly the circular cross section.

[25] The functional dependence $\langle D \rangle(r_h)$ is shown in Figure 9, where again the inset (note the linear scales) gives the results for the inner heliosphere. The fit through all averaged events is (D and r_h both in AU)

$$\langle D \rangle = (0.195 \pm 0.017) \cdot r_h^{(0.61 \pm 0.087)}, \tag{4}$$

and the result for the inner heliosphere is

$$\langle D \rangle = (0.23 \pm 0.05) \cdot r_h^{(1.14 \pm 0.44)}. \tag{5}$$

[26] The fit for the inner-heliospheric data follows approximately a linear increase of $\langle D \rangle$ with r_h. From the fitted equations, magnetic clouds expand faster in the inner heliosphere. The fit through all values overestimates the observed sizes at smaller distances, and the values obtained at larger distances than 1 AU show some variability around the fitted curve. The result is that MCs are growing fast after their release from the Sun, and their growth rate becomes less at larger heliospheric distances (>2 AU).

3.2.4. Density and Temperature

[27] A similar procedure is employed for the average proton density and temperature inside MCs, with the difference that these values are obtained from mean observed

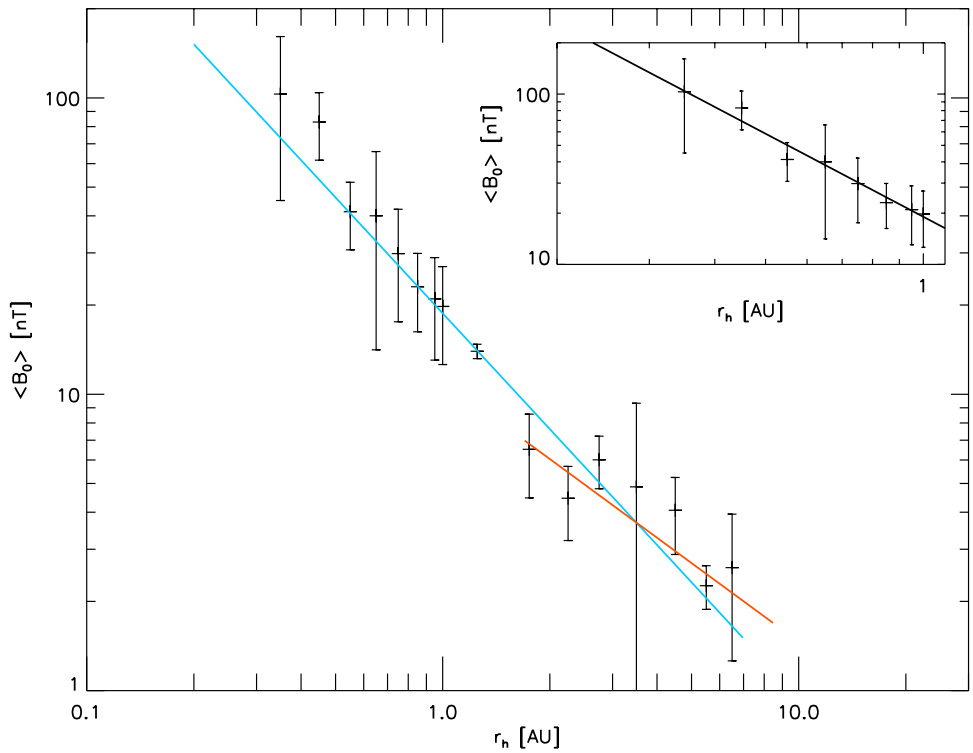

Figure 8. Double logarithmic plot of the fitted magnetic field strength inside magnetic clouds, averaged in each radial bin, versus heliospheric distance (mean values with standard deviation for each r_h-bin). The solid line in the big panel gives a weighted curve fit ($w = 1/\sigma^2$) through all values, and the shorter dashed line is a fit for $r_h > 2$ AU. The inset shows a fit using values in $r_h \leq 1$ AU.

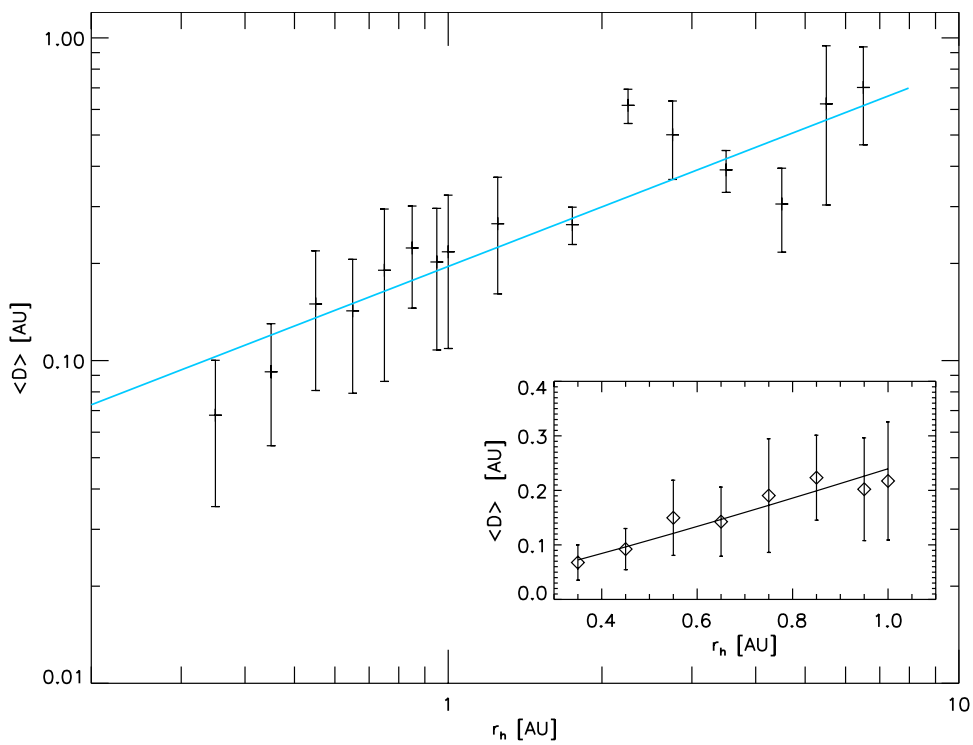

Figure 9. The average diameter of the magnetic cloud flux ropes versus heliospheric distance. Results in the inner heliosphere are shown on the inset (note the linear axes here). To obtain $\langle D \rangle$, the result from the least squares fit is taken into account and is used to correct the simple $v \cdot t$ relation, which gives the apparent diameter.

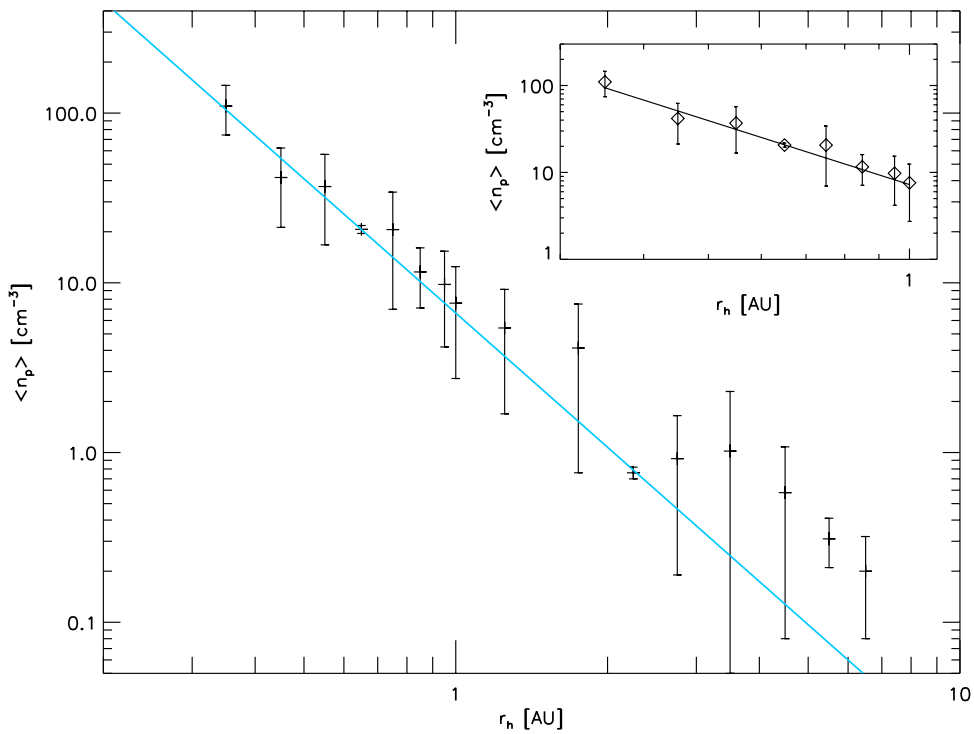

Figure 10. The variation with heliospheric distance of the average proton densities inside magnetic clouds.

values and no fit results are used to do corrections on these values. The behavior of these parameters is shown in Figures 10 and 11, respectively, where again a power law is fitted to all values and the values for the inner heliosphere. For the proton density we obtain,

$$\langle n_p \rangle = (6.63 \pm 0.28) \cdot r_h^{(-2.62 \pm 0.07)}, \tag{6}$$

and for the inner heliosphere

$$\langle n_p \rangle = (7.24 \pm 1.51) \cdot r_h^{(-2.44 \pm 0.46)}, \tag{7}$$

where n_p is in cm^{-3} and r_h in AU. For the ambient solar wind, the radial gradient for the density in the inner heliosphere using Helios observations only was found to be $n_p = 6.1 \cdot r_h^{-2.1}$ [*Schwenn*, 1990]. The exponent for MCs in the inner heliosphere is higher than those in the solar wind, confirming the notion that MC expand with respect to the ambient solar wind. From Figure 10 it can be seen that the mean values at distances greater than 1 AU have a tendency to lie above the fitted curve. This hump in the values is likely to be due to statistics, but nevertheless there is a difference in the drop between values up to 1 AU and beyond.

[28] For the proton temperature we obtain,

$$\langle T_p \rangle = (2.85 \pm 0.32) \cdot 10^4 \cdot r_h^{(-1.59 \pm 0.16)}, \tag{8}$$

and for the inner heliosphere

$$\langle T_p \rangle = (3.18 \pm 0.98) \cdot 10^4 \cdot r_h^{(-1.22 \pm 0.68)}, \tag{9}$$

with T_p in K and r_h in AU. We may compare the averages in equation (9) with the individual cases shown in Figures 1–3, at different r_h but all in the inner heliosphere. For these examples and using the nominal values for the constants in the temperature fit in the inner heliosphere, we obtain for the average temperatures $T_p = 1.0 \times 10^5$ K, 7.1×10^4 K, and 4.0×10^4 K, in good agreement with the observations. We now turn to the radial gradients in T_p. For r_h in the [0.3, 1.0] AU range, *Schwenn et al.* [1981] and *Marsch et al.* [1982] gave radial trends for the parallel and perpendicular proton temperatures. They obtained $T_{p,\parallel} \sim r_h^{-0.72}$ and $T_{p,\parallel} \sim r_h^{-1.00}$ for the fast (>400 km s^{-1}) and slow solar wind, respectively. The relations for the perpendicular temperature were $T_{p,\perp} \sim r_h^{-1.12}$ (fast wind) and $T_{p,\perp} \sim r_h^{-0.9}$ (slow wind). Considering $T_p = 1/3(2T_\perp + T_\parallel)$, all these relations, obtained from the Helios data sets, give a weaker decrease of T_p with radial distance than do the MCs. In the range 1–20 AU, many papers [see *Burlaga*, 1995, and references therein] obtained $T_p \sim r_h^{-a}$, where $0.5 \leq a \leq 0.7$, again much weaker than that found for MCs. Evidently, MCs cool faster than the ambient solar wind presumably because they expand relative to the wind.

3.2.5. Plasma β and Heliospheric Quasi-Invariant

[29] For the average plasma β, which is the ratio of the thermal pressure to the magnetic pressure, we find the following relationships:

$$\langle \beta \rangle = (0.043 \pm 0.007) \cdot r_h^{(-0.36 \pm 0.21)}, \tag{10}$$

and for the inner heliosphere

$$\langle \beta \rangle = (0.056 \pm 0.025) \cdot r_h^{(-0.08 \pm 0.57)}. \tag{11}$$

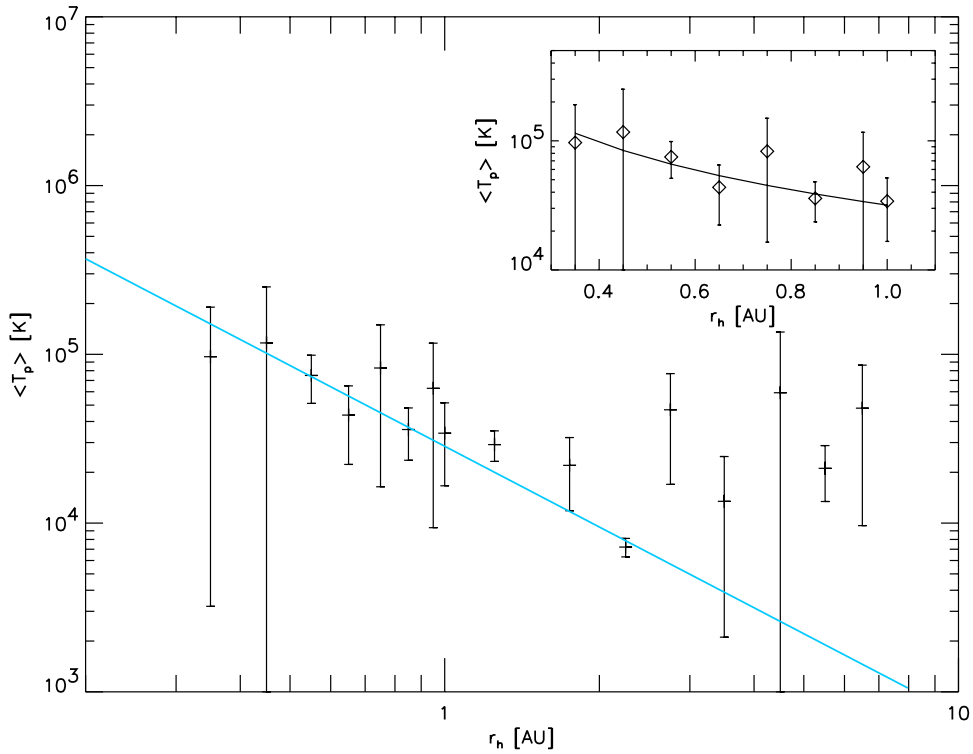

Figure 11. The variation with heliospheric distance of the average proton temperatures inside magnetic clouds.

The low plasma β is one of the criteria identifying MCs at 1 AU. The averaged β values of MCs at various heliospheric distances show that this low β criteria still holds for r_h within [0.3, 10] AU (see Figure 12). The nominal functional dependence in the inner heliosphere is weak but the error bar on the exponent is large. Because of the large error bars in the exponents in equations (10) and (11), it is doubtful whether the fit through all values has any significance, and it is

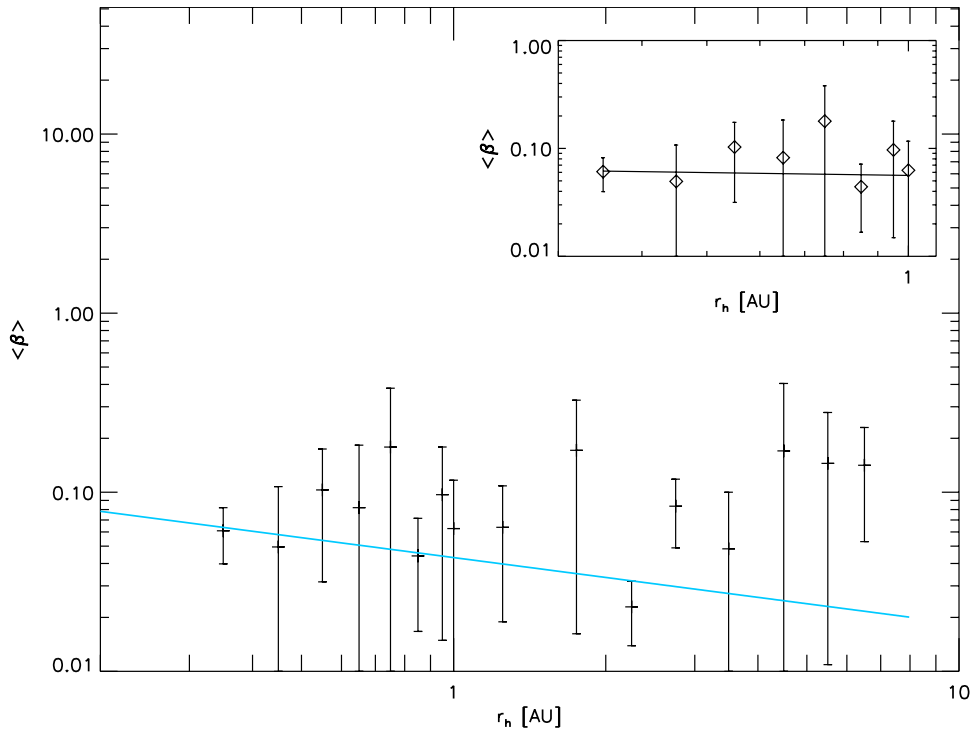

Figure 12. The average plasma β in magnetic clouds versus heliospheric distance.

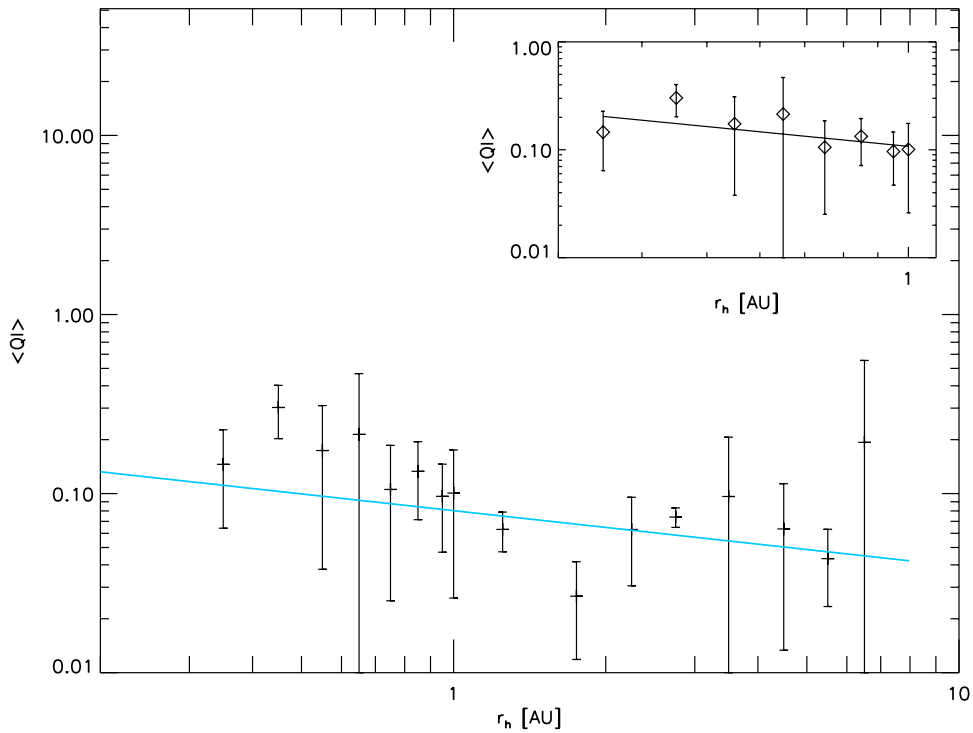

Figure 13. Average values of solar wind quasi-invariant, QI, inside magnetic clouds versus heliospheric distance.

included here only for completeness sake. The main point is that even considering the large error bars, the average proton β remains less than unity.

[30] Another important quantity which combines magnetic field and plasma parameters is the solar wind quasi-invariant, defined by *Osherovich et al.* [1999] as

$$QI \equiv \frac{B^2/8\pi}{\rho v^2/2} = M_A^{-2}, \tag{12}$$

where M_A is the Alfvén Mach number. Physically, QI represents the ratio of the magnetic to the plasma-kinetic energy densities. Its variation with r_h thus describes how the ratio of these important energy densities changes with distance from the Sun.

[31] Previous work [*Osherovich et al.*, 1999; *Fainberg et al.*, 2001] has shown that the quantity QI is a good proxy for solar activity, correlating well with a traditional index of solar activity, the sunspot number, both at 1 AU [*Osherovich et al.*, 1999] and at ~0.7 AU [*Fainberg et al.*, 2001]. An advantage of using QI is that, by contrast to indices based on remote observations of the solar disc, such as the sunspot number, it is a local index which follows quantitatively the propagation of solar activity through the heliosphere. In the inner heliosphere, that evolution is of direct import to studies of the geoeffects elicited by specific interplanetary configurations.

[32] Previous investigations of QI were done with measurements at 1 AU [*Osherovich et al.*, 1999], at the distance of Pioneer Venus Orbiter (0.72 AU; [*Fainberg et al.*, 2001]), and at large AUs [*Fainberg and Osherovich*, 2002]. *Leitner et al.* [2005a] were the first to use Helios observations to give the variation of QI with heliospheric distance, r_h. These measurements were for all the solar wind data and did not distinguish between solar wind structures. As an example, near the maximum of solar cycle 21 (1978), they obtained: QI = 0.027 r_h^{α}, where $\alpha = -1.12$ and -1.35 for Helios 1 and 2, respectively [*Leitner et al.*, 2005a, Table 1].

[33] Here we want to give results for the MCs alone. A study of the distribution of QI with r_h near solar maximum [see *Leitner et al.*, 2005a, Figure 2] shows the presence of "islands" detached from the main distribution and extending to higher values of QI than the general distribution. These are the magnetic clouds forming the tail of the distribution. The isolated high values result from the enhanced B-field strength in these ejecta [see also *Farrugia et al.*, 1995b].

[34] The way the relative energy densities inside magnetic clouds scale with heliospheric distance is found to be

$$\langle QI \rangle = (0.080 \pm 0.012) \cdot r_h^{(-0.31 \pm 0.18)} \tag{13}$$

and for the inner heliosphere

$$\langle QI \rangle = (0.107 \pm 0.033) \cdot r_h^{(-0.68 \pm 0.48)} \tag{14}$$

This quantity shows a clear trend to decline with increasing heliospheric distance, and a more rapid decrease is found for the inner heliosphere compared with values beyond 1 AU (Figure 13).

[35] By way of a general trend, let us compare the result for the inner heliosphere with that obtained by *Leitner et al.* [2005a] for the solar wind in 1976, when there were very few MCs. The result was QI = 0.015 $r_h^{-1.14}$ (Helios 1). This

Table 1. Selected Magnetic Cloud Events Which Are Observed By Two or More Spacecraft[a]

Event	Spacecraft	Year	DOY	r_h, AU	Long, deg	Lat, deg	B_0, nT	ϕ, deg	θ, deg	p	H	$\bar{B}_{tot}$, nT	D, AU
1a	IMP8	1974	285–287	1.00	20.6	0.0	26.62	117.4	−39.4	0.03	−1	19.33	0.356
1b	P11	1974	299–301	4.80	349.4	−1.4	5.86	93.8	4.8	0.05	−1	4.75	0.310
2a	H1	1975	321–321	0.87	50.1	0.0	16.81	99.2	−28.6	0.47	−1	12.09	0.118
2b	IMP8	1975	321–322	1.00	55.4	0.0	16.78	50.3	−18.1	0.22	−1	13.09	0.122
2c	P11	1975	332–333	3.77	42.0	11.3	2.63	131.5	−30.8	0.68	−1	1.68	-
3a	IMP8	1977	269–270	1.00	5.1	0.0	14.41	−93.0	−23.6	0.05	1	11.21	0.201
3b	V1	1977	270–271	1.06	11.3	0.5	13.66	−94.8	−17.6	0.09	1	10.55	0.224
3c	V2	1977	270–271	1.08	15.1	0.6	15.33	−176.2	−1.7	0.96	1	8.03	0.058
4a	IMP8	1977	329–330	1.00	64.9	0.0	19.28	108.7	3.6	0.46	−1	13.92	0.162
4b	H2	1977	328–328	0.62	56.2	0.0	33.34	92.3	4.5	0.06	−1	26.68	0.091
4c	V1	1977	332–333	1.58	62.0	1.0	9.63	75.0	−16.2	0.15	−1	6.88	0.214
4d	V2	1977	332–333	1.59	62.8	0.8	5.28	76.5	9.0	0.03	−1	4.17	0.171
5a	H2	1978	4– 5	0.94	98.9	0.0	25.86	−22.6	12.9	0.47	1	18.75	0.195
5b	OMNI2	1978	4– 5	1.00	104.6	0.0	19.94	−61.2	−16.4	0.15	1	14.40	0.376
5c	V1	1978	6– 7	1.98	78.8	1.0	6.46	−52.5	30.8	0.05	1	4.97	0.374
6a	H1	1978	60– 62	0.87	107.1	0.0	30.02	117.7	43.0	0.06	−1	22.08	0.357
6b	V1	1978	66– 68	2.56	93.7	1.0	5.99	41.0	11.7	0.65	−1	3.97	-
6c	V2	1978	66– 68	2.49	94.3	0.7	6.33	77.8	28.9	0.17	−1	4.81	0.622
7a	ISEE3	1980	79– 81	0.99	171	0.0	16.7	113.2	84.4	0.05	1	13.6	-
7b	Voy2	1980	108–109	6.4	162	1.8	1.0	95.8	50.9	0.00	1	0.92	-
7c	Voy1	1980	114–115	7.4	167	2.0	1.5	79.0	45.2	0.08	1	0.83	-
7d	P11	1980	127–131	9.4	181	6.2	1.3	97.8	41.9	0.00	1	-	-

[a]The beginning of the MC is given by year and DOY and the position of the spacecraft in solar ecliptic coordinates (radial distance and longitude and latitude). From the force-free field fit there results B_0, the magnetic field strength in the center of the cloud, θ and ϕ, the latitude and longitude of the axis, the impact parameter p, and the helicity H. The last two columns give the mean total magnetic field strength during the observation and the estimated diameter of the structure.

represents a more rapid decrease than for MCs and it also indicates that the QI index is dominated by the contribution of MCs. Typical values of the Alfven Mach number at 1 AU are 4 and 10 for MCs and solar wind, respectively [*Farrugia et al.*, 1995b], i.e., we would expect QI for MC to be about a factor of 6 higher, in general agreement with the results obtained here.

4. Spacecraft Lineups

[36] We now move on to the second step in which we complement the statistical results on $\langle B_0 \rangle$ presented above with direct spacecraft lineups. It is assumed that MCs propagate radially away from the Sun. Thus a perfect lineup is one when the same MC is observed by different spacecraft at different heliospheric distances and with a small difference in their longitude and latitude. Since most of the spacecraft have trajectories in the ecliptic plane ($\theta_{sc} \approx 0$), we searched for events where the difference in the longitude is small ($\Delta\phi_{sc} < 20°$). The spacecraft are thus well aligned because the trajectory relative to the MCs will be similar. The angular span of MCs can be as large as 60° [*Richardson and Cane*, 1993; *Marubashi*, 1997; *Bothmer and Schwenn*, 1998] so that our 20° criterion is a conservative one. If a MC drives a shock, the angular width of the shock is even bigger than the angular extent of the MC itself. Therefore it is possible that a shock which belongs to a MC is observed but not the MC itself.

[37] We developed an automated, interactive program to search for spacecraft alignments. When a MC is observed at one spacecraft, we search for other spacecraft which are within the range ($\Delta\theta \approx 0$ and $\Delta\phi < 20°$). We then determine if the event at these other spacecraft can be clearly identified as a MC in the observed temporal profiles. Table 1 lists some events which show a clear MC signature at different heliospheric distances. The columns give from left to right an index number, spacecraft identification, year, day of year, heliospheric distance, r_h, longitude and latitude, the fitted parameters B_0, ϕ, θ, p, and H, described in section 1, the observed total magnetic field, and the inferred diameter of the flux tube cross section. There are even more lineup events, but we concentrate on those which have a reliable fit result at all spacecraft in a given lineup, e.g., those with a low impact parameter p.

[38] As an example, Figure 14 shows Helios 1 observations of a magnetic cloud seen on DOY 61–62, 1978, at a heliospheric distance of 0.87 AU. The MC interval is bracketed by the second and third vertical guidelines. The red traces give the fit results. At this time, Voyager 2 is located at 2.49 AU. Taking the speed of the leading edge of the cloud as measured at Helios 1 of about 500 km s^{-1}, the cloud will require about 5.5 days to cover the 1.62 AU which separate the two spacecraft. The longitudinal separation between the two spacecraft is just 12.8° and while Helios 1 is in the ecliptic plane, Voyager 2 is just 0.7° above it. Figure 15 shows hourly values for the magnetic field and plasma parameters as observed by Voyager 2, plotted in the same format as in Figure 14 (but note that the timescales are different). The shock front which can be clearly seen in the Helios 1 data is observed at Voyager 2 as well at the end of DOY 64. While the typical signature of a magnetic cloud starts half a day after shock arrival at Helios 1, at the position of Voyager the cloud starts about one day after the onset of the shock. This indicates an expansion of the magnetosheath, itself a consequence of the expansion of the MC [*Erkaev et al.*, 1995; *Leitner et al.*, 2005b]. The fitted magnetic field strength is B_0 = 30.0 nT for Helios 1 and B_0 = 6.3 nT for Voyager 2, which implies a decrease with heliospheric distance proportional to $B_0 \propto r_h^{-1.48}$.

[39] Seven lineup events and fit results for each are given in Table 1. The data points in Figure 16 display the results obtained, with different lineups shown by different symbols.

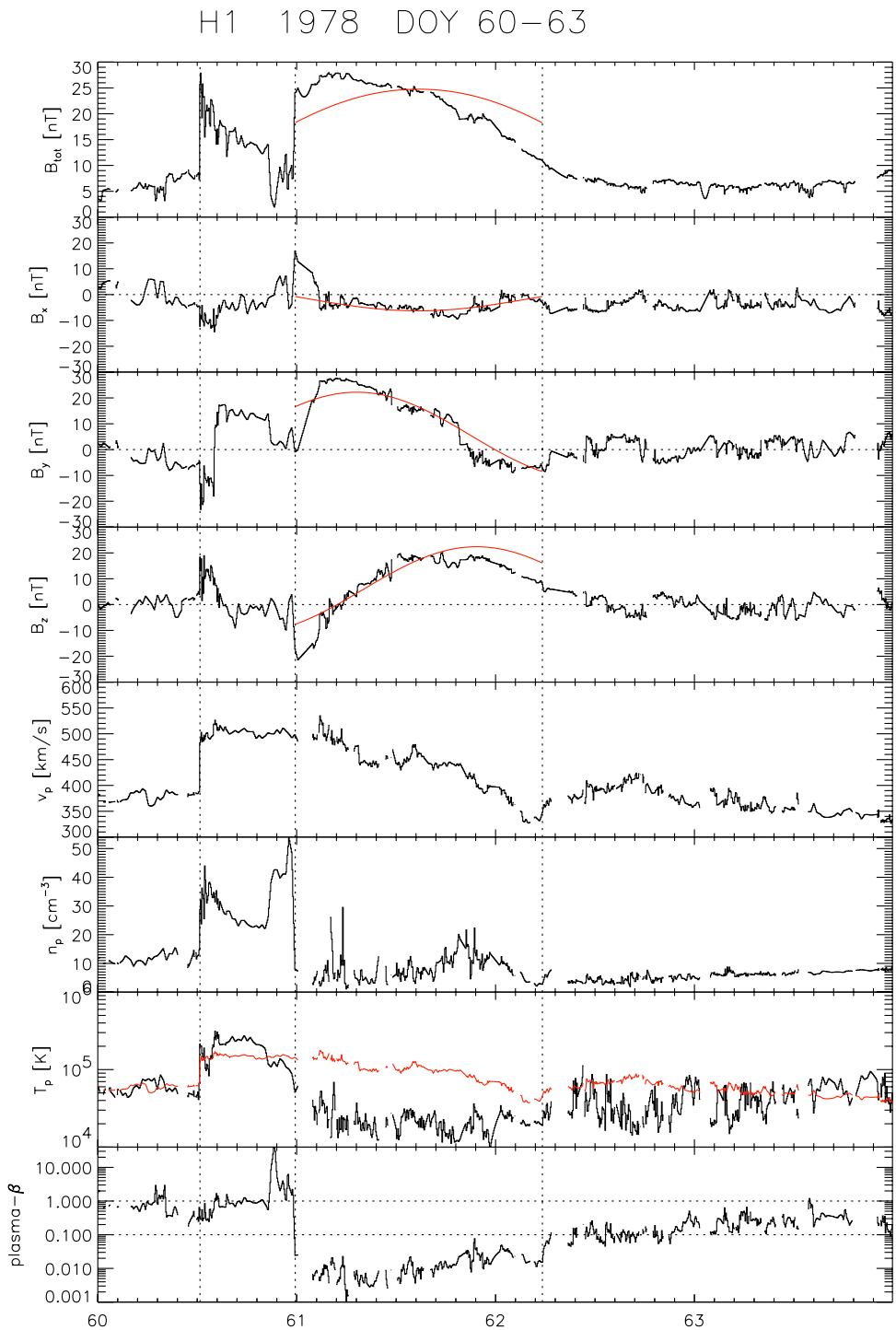

Figure 14. A magnetic cloud observed by Helios 1 at 0.87 AU. The fit result is shown by the red trace and is given also in Table 1.

The dashed line reproduces the statistical result obtained in the previous section for the inner heliosphere ($\langle B_0 \rangle \sim r_h^{-1.64}$), and the dotted line the statistical result at larger distances ($\langle B_0 \rangle \sim r_h^{-0.88}$). A generally good agreement may be seen. For most events, if we were to assume that the statistical decline with r_h in the inner heliosphere extends to higher r_h, most points in this range would lie above the line. This again is a hint that there is a different $B_0(r_h)$ dependence closer to the Sun and beyond 1 AU.

4.1. Expanding Lundquist Model

[40] Finally, we discuss the evolution of MCs through an analytical model for the freely expanding Lundquist magnetic flux rope. One motivation for studying this solution here is that *Zhao and Hoeksema* [1998] obtained better predictions as to the duration of a GSM B_z component using the expanding Lundquist solution than using the static one of *Lepping et al.* [1990]. (We use now the GSM system

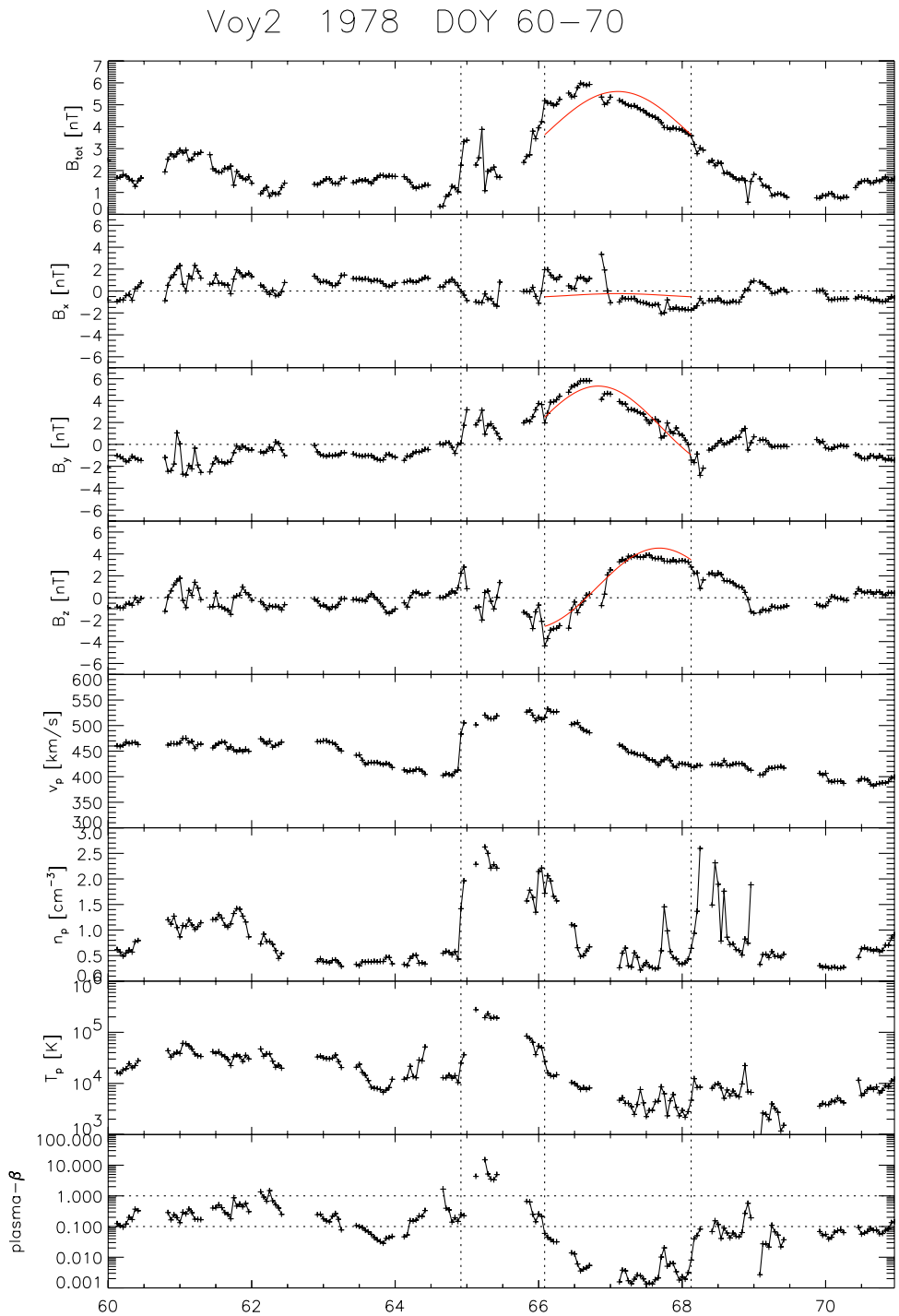

Figure 15. The same event as seen by Voyager 2 at ∼2.5 AU. Note the difference in the timescales.

because, while the IMF is ordered by a solar equatorial coordinate system, such as GSE, the interaction with the magnetosphere is controlled by a magnetospheric system, such as the GSM system.) Another is that the previous two approaches are based on static conditions. Yet another motivation is that this model attempted to explain at least some of the asymmetries in the total field profile, namely those in which the peak magnetic field strength is shifted toward the front edge, as a geometric effect resulting from expansion.

[41] The results obtained for a freely expanding Lundquist flux rope [*Farrugia et al.*, 1992, 1995a] are

$$\begin{aligned} B_{ax} &= \left(B_0/\tau^2\right) \cdot J_0(\alpha r/\tau), \\ B_\phi &= (B_0/\tau) \cdot J_1(\alpha r/\tau), \\ B_r &= 0, \end{aligned} \tag{15}$$

with B_{ax} and B_ϕ the axial and azimuthal components, respectively. Parameter $\tau = (t + t_0)/t_0$. Here, quantity t_0 is the

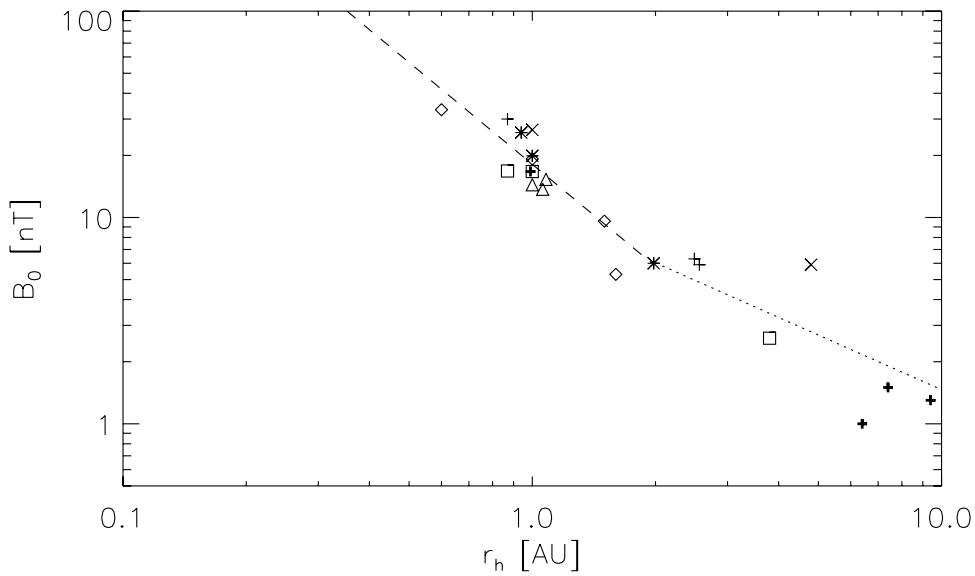

Figure 16. Fitted B_0 from the spacecraft alignments (Table 1). Alignment (1): x-sign, (2): squares, (3): triangles, (4): diamonds, (5): stars, (6): plus signs, (7): small plus signs. The dashed line is the dependence for the inner heliosphere obtained in the statistical survey; the dotted line represents the statistical result beyond 1 AU.

time from the start of expansion to the start of the observation at a given spacecraft situated at r_h, t is the time while the spacecraft is crossing the cloud, initialled to $t = 0$ on entry. B_0 is a constant for each observer.

[42] Let us discuss first the expansion of the cloud, $R(r_h)$. Suppose the front boundary of a MC reaches an observer. Then t = 0 and $\tau = 1$. The cloud radius at this time, i.e., at the first zero of J_0, when B_{ax} goes to zero, is $R(t_0) = 2.4/\alpha$. At time t, its radius $R(t)$ is given by $\alpha R(t)/\tau = 2.4$, i.e., $R(t) = R(t_0)\ \tau = R(t_0)\ ([t + t_0]/t_0)$. Assuming a constant speed of propagation, V_{MC}, we have from $t + t_0 = r_h/V_{MC}$ that $R(r_h) = [R(t_0)/V_{MC}t_0] \cdot r_h$. Thus the modeled radius of the flux tube increases linearly with heliospheric distance. To obtain an estimate of the constant of proportionality, consider representative values of the MC diameter ($2R(t_0)$) at $r_h = 1$ AU of $\approx$0.25 AU [*Klein and Burlaga*, 1982; *Bothmer and Schwenn*, 1998], or from the statistical result above for the inner heliosphere (equation (5)) of about 0.23 AU. These give $R = 0.12 \cdot r_h$. The linear rate of expansion predicted by this model is in good agreement with the statistical result for the inner heliosphere, for which we obtained an exponent of 1.14 (equation (5)), but represents a faster increase for $r_h > 1$ AU.

[43] We now discuss the maximum field strength $B_{\max}$ as measured by an observer as a function of r_h. We carry out a thought experiment and imagine a MC whose axis lies in the ecliptic and oriented exactly east-west. Suppose we place a set of observers along the Sun-Earth line in such a way that the front boundary passes over observer x, say, when its center is passing over the (more sunward placed) observer x-1. Let B_0 be numerically equal to 10 when this happens. Assume further that $t_0 = 1$ and $V_{MC} = 10$, numerically, when the front edge reaches observer x. For every time step, with $R(t) = R_0 \cdot \tau$, a new model field is calculated. Then, the relative position of the observer to the model is checked and a measurement is made. Figure 17, top, shows the field components B_{ax} (dashed line), B_ϕ (dotted line) and B_{total} (solid line) measured by x. The maximum field observed is $B_{\max} \approx 8.4$, and observer x crosses the cloud's axis (i.e. B_ϕ vanishes) at $t = 1.10$. This procedure is repeated for observer x + 1. The field components measured by $x + 1$ are as shown in Figure 17, bottom. The peak magnetic field strength is now $\approx$6.8, and the observer spends a longer time inside the cloud. Repeating this procedure for several successive observers, and noting the time when $B_{\max}$ is observed, we find the behavior of $B_{\max}$ shown in Figure 18, top. Since the cloud velocity is kept constant, the time $t + t_0$ on the abscissa is proportional to heliospheric distance r_h. After carrying out a power law fit to the data in Figure 18, top (solid line), we find that the peak magnetic field strength scales with r_h as $B_{\max} \propto r_h^{-2.0}$. The bottom of Figure 18 displays the linear expansion of the cloud radius derived above. In summary, it may be seen that this simple model predicts a faster decrease of $B_{\max}$ than we obtained from the statistical analysis, -2.0 versus -1.64 (inner heliosphere) and versus -1.30 full range of r_h.

5. Discussion and Conclusions

[44] We have presented a large-scale survey on the evolution of magnetic clouds using primarily data acquired by the Helios 1 and 2 probes in the range [0.3, 1.0] AU and by Wind in a similar phase of the solar cycle (ascending and maximum) two solar cycles later. These data sets were augmented by observations made by other spacecraft at large distances. The work aimed at drawing the consequences of adopting a widely used model of this subclass of interplanetary ejecta, in which these are considered as a cylindrically symmetric flux rope solutions of the force-free, constant-α magnetohydrodynamic equations, the solution of which was given first by *Lundquist* [1950]. From this model, we derived in a statistical approach the way various

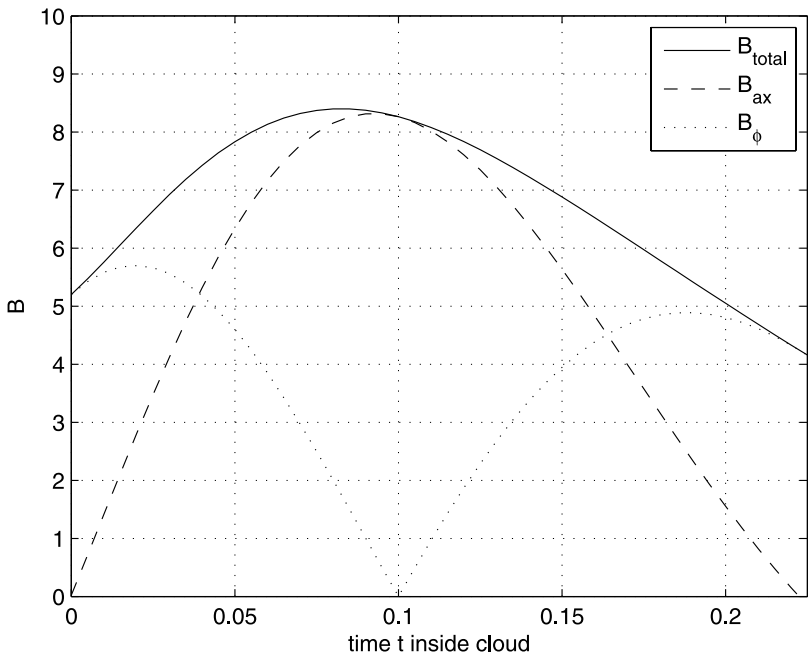

Figure 17a. The components of the magnetic field measured by the observer x: the axial field B_{ax} (dashed line), the azimuthal field B_{ϕ} (dotted line), and the total field, B_{total} (solid trace). For further details see text.

physical quantities (the model field strength on the tube axis, the diameter of the, assumed circular, cross section, its orientation, various plasma parameters, and a measure of the relative importance of the magnetic to plasma kinetic energy densities) depend on heliospheric distance, fitting the observations to power laws. The scaling laws of these quantities with distance from the Sun were derived in a statistical sense, both in the inner heliosphere, where the statistics are good, as well as for $1 < r_h < 7$ AU. Through direct observations of some of these quantities at two or more locations in approximate alignment, we could follow their evolution in snapshot fashion. Finally, we considered an analytical expression for the freely expanding Lundquist tube and derived its predictions concerning the growth of the flux tube's diameter and the decline of its central magnetic field strength. We now (1) take a critical look at our assumptions, (2) compare with previous work in this area, and (3) mention the import of this study on inves-

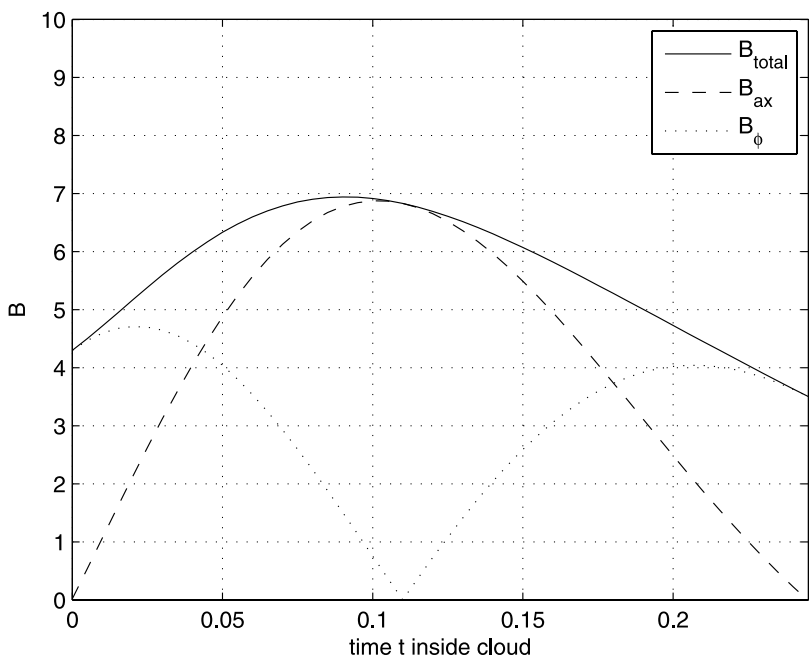

Figure 17b. Similar to Figure 17a, but now showing the field components measured by observer $x + 1$.

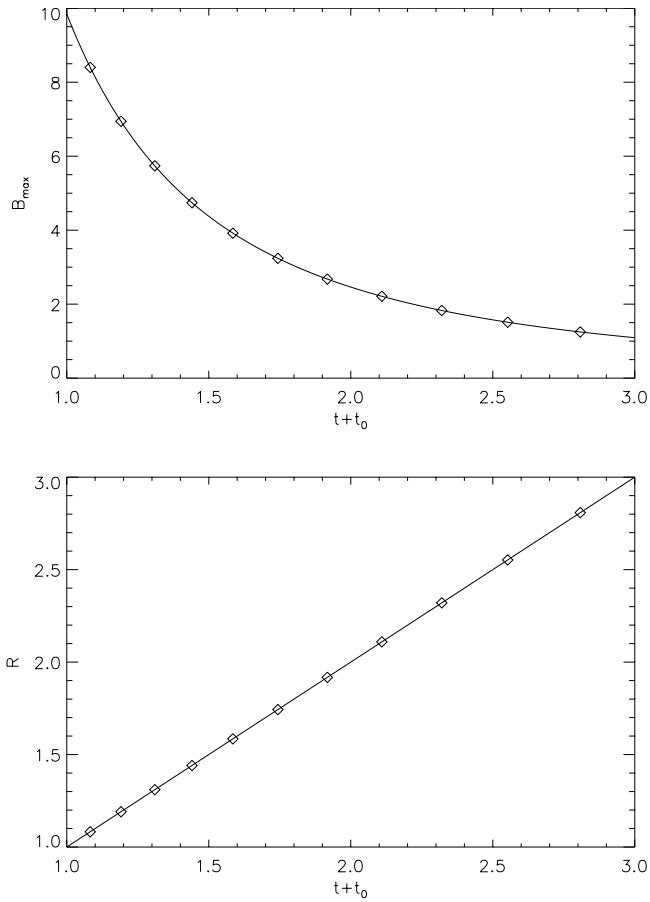

Figure 18. The top panel shows the decrease of the maximum field strength with $t_0 + t$, a quantity proportional to the heliospheric distance, r_h. The bottom panel gives the corresponding result for the size of the expanding tube.

tigations of the geomagnetic effects, in particular the ability to predict magnetospheric disturbances from afar.

[45] Our approach is based on a specific geometry, i.e., the circular cross section of the magnetic flux rope. Therefore for example, the values of D(r_h) are not only obtained by a simple $V_{MC} \cdot t$ relation derived directly from observations but partly from the fit (via the impact parameter and flux rope orientation) and partly from the geometry. Interestingly, the relation we obtain has the largest scatter compared to, say, the fit result for B_0. This is true of both the statistical results in section 3.2.3 as well as of the spacecraft line-up observations (not shown). This might reflect a departure from the circular cross section of the flux tube assumed in the calculation of D.

[46] In recent work, the "circular cross section" assumption has been questioned from at least three aspects. In early work [*Gosling*, 1990], the configuration was often suggested to be that of a plasmoid detached from the Sun, perhaps with the same field line topology as the classical spheromak [*Rosenbluth and Bussac*, 1979; *Farrugia et al.*, 1995a]. This model is now little espoused, since many studies have shown continued connection of the "feet" of magnetic clouds to the Sun [e.g., *Farrugia et al.*, 1993a, 1993b]. In work attempting to reconstruct the magnetic field, orientation of the flux tube, etc., based on solutions of the Grad-Shafranov equation, *Hu and Sonnerup* [2002] present two examples in which they infer substantial deviations from this geometry. Finally, studying kinematic expansions of magnetic clouds, *Riley and Crooker* [2004] propose a shape which becomes increasingly flattened as r_h increases ("pancake" shape). A full-scale investigation which gets rid of the underlying geometrical presumptions, while retaining the static assumptions, is under way and will be reported elsewhere.

[47] We emphasized the inner-heliospheric evolution, giving separate results on the scaling factors for $r_h \leq 1$. First, our data here are very extensive, so the statistics are good. Second, we did this because clearly the inner-heliospheric evolution is the most relevant one when investigating the geomagnetic consequences. On this issue, we discuss briefly two points. All so-called "coupling functions," which aim at expressing the fraction of energy and momentum extracted from the solar wind by the magnetosphere, depend on interplanetary quantities we have been discussing. For example, the traditional and widely used Akasofu ϵ parameter, $\epsilon = 1/\mu_0\, VB^2 \sin^4(\theta/2)$ (θ = clock angle, i.e., the polar angle in the GSM *YZ* plane [*Perreault and Akasofu*, 1978]), giving the fraction of the Poynting flux entering the magnetosphere per unit area [*Farrugia et al.*, 1993a, 1993b; *Freeman and Farrugia*, 1999], depends crucially on the strength of the magnetic field squared, thus being very sensitive to scaling.

[48] One remarkable example of predictions of geomagnetic effects from measurements made by distant probes is the attempt by *Lindsay et al.* [1999] to predict the ring current enhancement (as measured by the D_{st} index) over long periods using measurements made by ISEE 3 at 1 AU, by Pioneer Venus orbiter (PVO) at about 0.7 AU, and by Helios 1. PVO data would furnish a prediction with a typical lead time of about 1 day. Using the *Burton et al.* [1975] formula for the temporal development of the D_{st}, they achieve quite good agreement. Interestingly, the disagreement between observed and predicted D_{st} appears strongest in the larger disturbances, i.e., precisely those we would like to predict most reliably. The magnetic field strength in this study is scaled as r_h^{-1}. Our inner-heliopsheric dependence for this quantity follows, rather, a $r_h^{-1.64}$ dependence, i.e., a faster decrease. It is well worth checking whether with such a dependence the predictions would not be more in agreement with the observations.

[49] The lineup results on MC evolution presented in section 4 were in the nature of snapshots, i.e., two results of a static model on the same magnetic cloud made at different heliospheric distances. Such results are somewhat limited in what they can assert on the evolution. Furthermore, the lineups were few in number. Yet, snapshots made sometimes at a time difference of 1 week or more do let us infer the changes which have taken place in the intervening period of time when no observations are available. We find it remarkable that, despite some difference in the results from those of the statistical approach, the similarities are strong.

[50] An investigation much broader in scope than our concerns here but yet overlapping with ours was undertaken by *Bothmer and Schwenn* [1998]. We note that the approaches and aims here and in that study are different. Thus for

instance, the orientation of the cloud axis is obtained in that study by minimum variance analysis [*Sonnerup and Cahill* [1967], whereas here we carry out least squares fits to a specific model. Also, the diameter of the tube was obtained there from the observations, i.e., the apparent diameter, and takes no account of the distance that the spacecraft trajectory passes from the cloud's center and from the tube's orientation. The size of the cloud was obtained there as (in our notation)

$$D(r_h) = (0.24 \pm 0.01) \times r_h^{0.78\pm0.1}, \qquad (16)$$

with r_h in AU. In our study the MCs are growing faster in the inner heliosphere. Our statistical result on the density, which is obtained purely from data, is in agreement with the *Bothmer and Schwenn* [1998] study. There are small differences between the orientations obtained from the minimum variance method and the force-free field method, and it is our future aim to check whether there is a systematic difference between these two models.

[51] This work has an import on future NASA missions. We think in particular of the Sentinels initiative within the Living with a Star program and the Solar Terrestrial Relations Observatory (STEREO) mission. The primary objective of Sentinels is to discover, understand, and model the connection between solar phenomena and interplanetary disturbances, particularly those with an impact on geospace. Magnetic clouds are such disturbances, and a scientific aim of this mission is to investigate the evolution of magnetic clouds in the inner heliosphere. The suite of spacecraft will orbit much like Helios, only they will spend relatively longer times at small r_h. We feel that the work we presented here will form a good starting point for the investigations to be undertaken by the Sentinels mission. The work here should also form a useful background to the STEREO mission, one of whose scientific objectives is to employ its three-dimensional capabilities to track the motion of ejecta and MCs through space.

[52] **Acknowledgments.** We are grateful to the referees for their many helpful comments. We thank R.P. Lepping for the Wind magnetic field data used in this study. We thank the National Space Science Data Center (NSSDC) for providing the data sets for ISEE–3, P10, P11, PVO, V1, and V2. This work is supported by the Austrian "Fonds zur Förderung der wissenschaftlichen Forschung" under project P17100-N08, NASA Wind/SWE, and MFI grant NNG05GC75G, NASA grant NNG06GD41G, and NASA STEREO grant NAS5-00132. Support was given from the Austrian Academy of Sciences, "Verwaltungsstelle für Auslandsbeziehungen," while CJF was on a visit in Graz and while ML was on a visit in Krasnojarsk.

[53] Zuyin Pu thanks Volker Bothmer and Katsuhide Marubashi for their assistance in evaluating this paper.

References

Bothmer, V. (2003), Sources of magnetic helicity over the solar cycle, in *Proceedings of ISCS 2003 Symposium: Solar Vaiability as an Input to the Earth's Environment*, *Eur. Space Agency Spec. Publ.*, *ESA SP-535*, 419–428.

Bothmer, V., and R. Schwenn (1996), Signatures of fast CMEs in interplanetary space, *Adv. Space Res.*, *17*, 319–322.

Bothmer, V., and R. Schwenn (1998), The structure and origin of magnetic clouds in the solar wind, *Ann. Geophys.*, *16*, 1–24.

Burlaga, L. F. (1988), Magnetic clouds and force–free fields with constant alpha, *J. Geophys. Res.*, *93*, 7217–7224.

Burlaga, L. F. (1995), *Interplanetary Magnetohydrodynamics*, Oxford Univ. Press, New York.

Burlaga, L. F., E. Sittler, F. Mariani, and R. Schwenn (1981), Magnetic loop behind an interplanetary shock: Voyager, Helios and IMP 8 observations, *J. Geophys. Res.*, *86*, 6673–6684.

Burlaga, L. F., L. Klein, N. R. Sheeley Jr., D. J. Michels, R. A. Howard, M. J. Koomen, R. Schwenn, and H. Rosenbauer (1982), A magnetic cloud and a coronal mass ejection, *Geophys. Res. Lett.*, *9*, 1317–1320.

Burton, R. K., R. L. McPherron, and C. T. Russell (1975), An empirical relationship between interplanetary conditions and *Dst*, *J. Geophys. Res.*, *80*, 4204–4214.

Erkaev, N. V., C. J. Farrugia, H. K. Biernat, L. F. Burlaga, and G. A. Bachmaier (1995), Ideal MHD flow behind interplanetary shocks driven by magnetic clouds, *J. Geophys. Res.*, *100*, 19,919–19,931.

Fainberg, J., and V. A. Osherovich (2002), Solar wind quasi-invariant as a heliospheric index of solar activity, in *Proceedings of 10th European Solar Physics Meeting "Solar Variability: From Core to Outer Frontiers," Eur. Space Agency Spec. Publ.*, *ESA SP-506*, 43.

Fainberg, J., V. A. Osherovich, and R. G. Stone (2001), Pioneer Venus Orbiter observations of a solar wind quasi-invariant, *Geophys. Res. Lett.*, *28*, 1447–1449.

Fainberg, J., V. A. Osherovich, and R. G. Stone (2001), Pioneer Venus Orbiter observations of solar wind quasi-invariant, *Geophys. Res. Lett.*, *28*, 1447–1450.

Farrugia, C. J., L. F. Burlaga, V. A. Osherovich, and R. P. Lepping (1992), A comparative study of dynamically expanding force-free, constant-alpha magnetic configurations with applications to magnetic clouds, in *Solar Wind Seven*, edited by E. Marsch and R. Schwenn, pp. 611, Pergamon, New York.

Farrugia, C. J., I. G. Richardson, L. F. Burlaga, V. A. Osherovich, and R. P. Lepping (1993a), Simultaneous observations of solar MeV particles in a magnetic cloud and in the Earth's northern tail lobe: Implications for the global field line topology of magnetic clouds and for the entry of solar particles into the magnetosphere during cloud passage, *J. Geophys. Res.*, *98*, 15,497–15,507.

Farrugia, C. J., L. F. Burlaga, V. Osherovich, I. G. Richardson, M. P. Freeman, R. P. Lepping, and A. Lazarus (1993b), A study of an expanding interplanetary magnetic cloud and its interaction with the the Earth s magnetosphere: The interplanetary aspect, *J. Geophys. Res.*, *98*, 7621–7632.

Farrugia, C. J., V. A. Osherovich, and L. F. Burlaga (1995a), Magnetic flux rope versus the spheromak as models for interplanetary magnetic clouds, *J. Geoophys. Res.*, *100*, 12,293–12,306.

Farrugia, C. J., N. V. Erkaev, H. K. Biernat, and L. F. Burlaga (1995b), Anomalous magnetosheath properties during Earth passage of an interplanetary magnetic cloud, *J. Geophys. Res.*, *100*, 19,245–19,258.

Freeman, M. P., and C. J. Farrugia (1999), Solar wind input between substorm onsets during and after the October 18–20, 1995, magnetic cloud, *J. Geophys. Res.*, *104*, 22,729–22,744.

Goldstein, H. (1983), On the field configuration in magnetic clouds, in *Solar Wind Five*, edited by M. Neugebauer, *NASA Conf. Publ.*, *CP-2280*, 731.

Gosling, J. T. (1990), Coronal mass ejections and magntic flux ropes in interplanetary space, in *Physics of Magnetic Flux Ropes*, *Geophys. Monogr. Ser.*, vol. 58, edited by E. R. Priest, L. C. Lee, and C. T. Russell, pp. 343–354, AGU, Washington, D. C.

Howard, R. A., N. R. Sheeley Jr., D. J. Michels, and M. J. Koomen (1986), The solar cycle dependence of coronal mass ejections, in *The Sun and the Heliosphere in Three Dimensions*, edited by R. G. Marsden, p. 107, D. Reidel, Norwell, Mass.

Hu, Q., and B. U. Ö. Sonnerup (2002), Reconstruction of magnetic clouds in the solar wind: Orientation and configuration, *J. Geophys. Res.*, *107*(A7), 1142, doi:10.1029/2001JA000293.

Huttunen, K. E. J., R. Schwenn, V. Bothmer, and H. E. J. Koskinen (2005), Properties and geoeffectiveness of magnetic clouds in the rising, maximum and early declining phases of solar cycle 23, *Ann. Geophys.*, *23*, 625–641.

Klein, L. W., and L. F. Burlaga (1982), Interplanetary magnetic clouds at 1 AU, *J. Geophys. Res.*, *87*, 613–624.

Leitner, M., C. J. Farrugia, V. A. Osherovich, J. Fainberg, H. K. Biernat, K. W. Ogilvie, R. Schwenn, and R. Torbert (2005a), The relative distributions of the magnetic and plasma kinetic energy densities in the inner heliosphere (<1 AU), *Solar Wind 11*, edited by B. Fleck and T. H. Zurbuchen, *Eur. Space Agency Spec. Publ.*, *ESA SP-592*, 743-746.

Leitner, M., C. J. Farrugia, H. K. Biernat, R. Torbert, N. V. Erkaev, K. W. Ogilvie, and R. Schwenn (2005b), On the thickness of the sheath of magnetic clouds in the inner heliopshere: A Helios–Wind Investigation, *Solar Wind 11*, edited by B. Fleck and T. H. Zurbuchen, *Eur. Space Agency Spec. Publ.*, *ESA SP-592*, 739-742.

Lepping, R. P., J. A. Jones, and L. F. Burlaga (1990), Magnetic field structure of interplanetary magnetic clouds at 1 AU, *J. Geophys. Res.*, *95*, 11,957–11,965.

Lindsay, G. M., C. T. Russell, and J. G. Luhmann (1999), Predictability of Dst index based upon solar wind conditions monitored inside 1 AU, *J. Geophys. Res.*, *104*, 10,335–10,344.

Lopez, R. E., and J. W. Freeman (1986), Solar wind proton temperature-velocity relationship, *J. Geophys. Res.*, *91*, 1701–1705.

Lundquist, S. (1950), Magneto–hydrostatic fields, *Ark. Fys*, *2*, 361–365.

Marsch, E., K.-H. Muehlhaeuser, R. Schwenn, H. Rosenbauer, W. G. Pilipp, and F. M. Neubauer (1982), Solar wind protons: Three-dimensional velocity distributions and derived parameters measured between 0.3 and 1 AU, *J. Geophys. Res.*, *87*, 52–72.

Mariani, F., and F. M. Neubauer (1990), The interplanetary magnetic field, in *Physics of the Inner Heliosphere*, vol. I, edited by R. Schwenn and E. Marsch, p. 183, Springer, New York.

Marubashi, K. (1997), Interplanetary magnetic flux ropes and solar filaments, in *Coronal Mass Ejections*, *Geophys. Monogr. Ser.*, vol. 99, edited by N. Crooker, J. Joselyn, and J. Feyman, pp. 147–156, AGU, Washington, D. C.

Osherovich, V. A., C. J. Farrugia, and L. F. Burlaga (1993), Dynamics of aging magnetic clouds, *Adv. Space Res.*, *13*(6), 57.

Osherovich, V. A., J. Fainberg, and R. G. Stone (1999), Solar wind quasi-invariant as a new index of solar activity, *Geophys. Res. Lett.*, *26*, 2597–2600.

Perreault, P., and S.-I. Akasofu (1978), A study of geomagnetic storms, *Geophys. J. R. Astron. Soc.*, *54*, 547–573.

Press, W. H., S. A. Teukolsky, W. H. Vetterling, and B. P. Flannery (1982), *Numerical Recipes in Fortran 77*, 2nd ed., Cambridge Univ. Press, New York.

Richardson, I. G., and H. V. Cane (1993), Signatures of shock drivers in the solar wind and their dependence on the solar source location, *J. Geophys. Res.*, *98*, 15,295–15,304.

Riley, P., and N. U. Crooker (2004), Kinematic treatment of coronal mass ejection evolution in the solar wind, *Astrophys. J.*, *600*, 1035–1042.

Rosenbluth, M. N., and M. N. Bussac (1979), MHD stability of spheromak, *Nucl. Fusion*, *19*, 489.

Schwenn, R. (1983), The average solar wind in the inner heliosphere: Structures and slow variations, in *Solar Wind Five*, edited by M. Neugebauer, *NASA Conf. Publ.*, *CP-2280*, page numbers?.

Schwenn, R. (1990), Large-scale structure of the interplanetary medium, in *Physics of the Inner Heliosphere*, vol. I, edited by R. Schwenn and E. Marsch, p. 99, Springer, New York.

Schwenn, R., K.-H. Muehlhaeuser, E. Marsch, and H. Rosenbauer (1981), Two states of the solar wind at the time of solar activity minimum, 2, Radial gradients of plasma parameters in fast and slow streams, *Solar Wind 4*, edited by H. Rosenbauer, *Rep. MPAE-W-100-81-31*, p. 126, Max-Planck-Inst. für Aeron., Katlenburg-Lindau, Germany.

Sonnerup, B. U. Ö., and L. J. Cahill (1967), Magnetopause structures and attitude from Explorer 12 observations, *J. Geophys. Res.*, *72*, 171–183.

Tsurutani, B. T., et al. (2004), Properties of slow magnetic clouds, *J. Atmos. Sol. Terr. Phys.*, *66*, 147–151.

Webb, D. F., and R. A. Howard (1994), The solar cycle variation of coronal mass ejections and the solar wind mass flux, *J. Geophys. Res.*, *99*, 4201.

Zhao, X. P., and J. T. Hoeksema (1998), Central axial field direction in magnetic clouds and its relation to southward interplanetary magnetic field events and dependence on disappearing solar filaments, *J. Geophys. Res.*, *103*, 2077–2084.

Zhao, X. P., J. T. Hoeksema, and K. Marubashi (2001), Magnetic cloud B_s events and their dependence on cloud parameters, *J. Geophys. Res.*, *106*, 15,643–15,643.

H. K. Biernat, M. Leitner, and C. Möstl, Space Research Institute, Austrian Academy of Sciences, Schmiedlst. 6, A-8042 Graz, Austria. (martin.leitner@oeaw.ac.at)

C. J. Farrugia and A. B. Galvin, Space Science Center and Department of Physics, University of New Hampshire, College Road, Durham, NH 03824, USA.

K. W. Ogilvie, Laboratory for Extraterrestrial Physics, NASA Goddard Space Flight Center, Greenbelt Road, Greenbelt, MD 20771, USA.

R. Schwenn, Max Planck Institute for Solar System Research, Max-Planck Str., Katlenburg-Lindau, D-3791, Germany.